약학박사 학위논문

비스테로이드성 항염증제에 의한 간의 지질대사 이상에서 소포체 스트레스와 샤페론-매개 자가포식의 역할

Role of ER stress and chaperone-mediated autophagy in NSAID-induced impairment of hepatic lipid metabolism

2022 년 8 월

서울대학교 대학원

약학과 예방약학 전공

이 원 석

Role of ER stress and chaperone-mediated autophagy in NSAID-induced impairment of hepatic lipid metabolism

비스테로이드성 항염증제에 의한 간의 지질대사 이상에서
소포체 스트레스와 샤페론-매개 자가포식의 역할

지도교수 이 병 훈

이 논문을 약학박사 학위논문으로 제출함
2022년 7 월

서울대학교 대학원
약학과 예방약학 전공
이 원 석

이원석의 박사 학위논문을 인준함
2022년 8 월

위 원 장 창 동 신 (인)
부위원장 이 미 옥 (인)
위 원 이 병 훈 (인)
위 원 차 혁 진 (인)
위 원 강 동 민 (인)

Abstract

While some non-steroidal anti-inflammatory drugs (NSAIDs) are reported to induce hepatic steatosis, the molecular mechanisms are poorly understood. This study presents the mechanism by which NSAIDs induce hepatic lipid accumulation. Degradation of lipid droplet protein, PLIN2, by chaperone-mediated autophagy (CMA) is critical for the initiation of lipid mobilization. NSAIDs tested in this study accumulated neutral lipid in hepatic cells. Diclofenac demonstrated the most potent effect on lipid accumulation. Diclofenac-induced lipid accumulation was confirmed in primary mouse hepatocytes and the liver of mice. NSAIDs inhibited CMA activity by inducing the decreased expression of lysosome-associated membrane glycoprotein 2 isoform A (LAMP2A) protein. The expression of CMA substrate proteins including PLIN2 increased, and the activity of photoactivable KFERQ-PAmCherry reporter decreased after diclofenac treatment in HepG2 cells. Reactivation of CMA by treatment with AR7 or overexpression of LAMP2A inhibited diclofenac-induced lipid accumulation and hepatotoxicity. Diclofenac treatment upregulated SNX10 via CHOP-dependent ER stress response. The increase of SNX10 induced the maturation of cathepsin A and the lysosomal degradation of LAMP2A. Thus, these results demonstrated that NSAIDs induce SNX10- and CTSA-dependent degradation of LAMP2A, thereby leading to the suppression of CMA. The CMA impairment decreases the degradation of PLIN2 and disrupts cellular lipid homeostasis, leading to NSAID-induced steatosis and hepatotoxicity.

Keywords: Chaperone-mediated autophagy; Diclofenac; Lipid metabolism; NSAIDs; Perilipin 2; Sorting nexin 10
Student Number: 2015-21890

Contents

List of Figures

List of Abbreviations

Bip (GRP78) : Binding immunoglobulin protein (the glucose-regulated protein-78)

BODIPY 493/503 :

4,4-Difluoro-1,3,5,7,8-pentamethyl-4-bora-3a,4a-diaza-s-indacene

CHOP : C/EBP homologous protein

COX : Cyclooxygenase

CMA : Chaperone-mediated autophagy

CTSA : Cathepsin A

ER : Endoplasmic reticulum

GAPDH: Glyceraldehyde 3-phosphate dehydrogenase

HSC70 : Heat shock cognate 71 kDa protein

LAMP : Lysosomal associated membrane protein

LD : Lipid droplet

MPH : Mouse primary hepatocytes

NAFLD : Non-alcoholic fatty liver disease

NSAID : Non-steroidal anti-inflammatory drug

PLIN : Perilipin

PK : Pyruvate kinase

ROS : Reactive oxygen species

SNX10 : Sorting nexin 10

TG : Triglyceride

1. Introduction

1.1. Adverse effects of nonsteroidal anti-inflammatory drugs (NSAIDs)

1.1.1. Hepatotoxicity of NSAIDs

Non-steroidal anti-inflammatory drugs (NSAIDs) are one of the most widely used analgesic and anti-inflammatory agents worldwide. Although gastrointestinal adverse events are most common, hepatic injury is another unintended consequence of NSAIDs use (Schmeltzer *et al.,* 2016). In fact, NSAIDs including bromfenac, ibufenac, and benoxaprofen have been withdrawn from the market due to fatal cardiovascular and hepatic toxicity (Bessone, 2010).

The estimated incidence of NSAID-induced hepatotoxicity is variable, ranging from 0.29 to 9 cases per 100,000 patients per year (Schmeltzer *et al.,* 2019). NSAIDs have also been ranked as the fourth leading cause of drug-induced liver injury (12.5% of total reported cases), following anti-infectious (34.9%), cardiovascular (17.3%), and psychotropic (13.1%) medications (Sarah Low *et al.,* 2020) (Figure 1).

Recent papers reported that 99% of reported cases of hepatotoxicity are caused by seven NSAIDs (Meunier *et al.*, 2018). Most of the NSAIDs belong to two groups, acetic acid derivatives (46.5%) and propionic acid derivatives (25.7%) (Agúndez *et al.,* 2011) (Table 1).

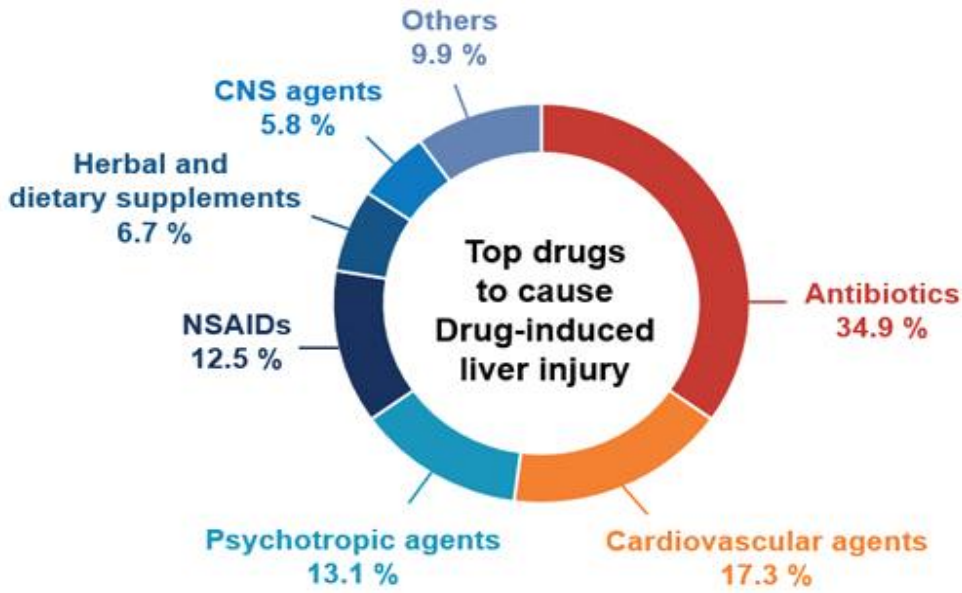

Figure 1. The ranking of causative events implicated in drug-induced liver injury (Sarah Low *et al.,* 2020)

Group	Generic name	Percentage of tatal cases of live injury (NSAIDs)
Acetic acid derivatives	Aceclofenac	< 0.1%
	Acemetacin	< 0.1%
	Diclofenac	34.1%
	Indomethacin	< 0.1%
	Ketorolac	< 0.1%
	Sulindac	12.4%
Propionic acid derivatives	Dexketoprofen	< 0.1%
	Ibuprofen	8.4%
	Ketoprofen	< 0.1%
	Naproxen	6.4%
	Oxaprozin	< 0.1%
Enolic acid derivatives	Droxicam	< 0.1%
	Meloxicam	< 0.1%
	Piroxicam	9.3%
	Tenoxicam	< 0.1%
Salicylates	Aspirin	12.0%
	Salsalate	< 0.1%
Selective COX-2 inhibitors	Celexocib	< 0.1%
	Rofecoxib	< 0.1%
	Valdecoxib	< 0.1%
Sulfonanilides	Nimesulide	5.8%

Table 1. NSAIDs in common use which cause hepatotoxicity. (Agúndez *et al.,* 2011)

1.1.2. NSAID-induced hepatic steatosis

Drug-induced steatosis is primarily mediated by interference with mitochondrial respiration and β-oxidation of hepatocytes. When hepatic mitochondrial β-oxidation is severely impaired, the level of fatty acyl-CoA and nonesterified fatty acids are increased. These metabolites are ultimately converted into TGs, resulting in hepatic steatosis. In addition, intracellular TG level increases when the carnitine palmitoyl shuttle-mediated entry of long-chain free fatty acid is inhibited. The increased free fatty acids in the cytosol are esterified into TGs (Patel *et al.,* 2013) (Figure 2).

Most NSAIDs with hepatotoxicity cause steatosis or steatohepatitis with pathological features resembling those of alcoholic fatty liver disease or non-alcoholic fatty liver disease (NAFLD). Mitochondrial damage and the generation of reactive oxygen species (ROS) are the key initiating events associated with NSAID-induced hepatotoxicity and hepatic steatosis (Gómez-Lechón *et al.,* 2003; Al-Attrache *et al.,* 2016). Some NSAIDs have been reported to induce hepatic steatosis, including some fatal cases, by inhibiting mitochondrial β-oxidation of fatty acids irrespective of their cyclooxygenase (COX)-inhibiting properties (Geneve *et al.,* 1987; Freneaux *et al.,* 1990).

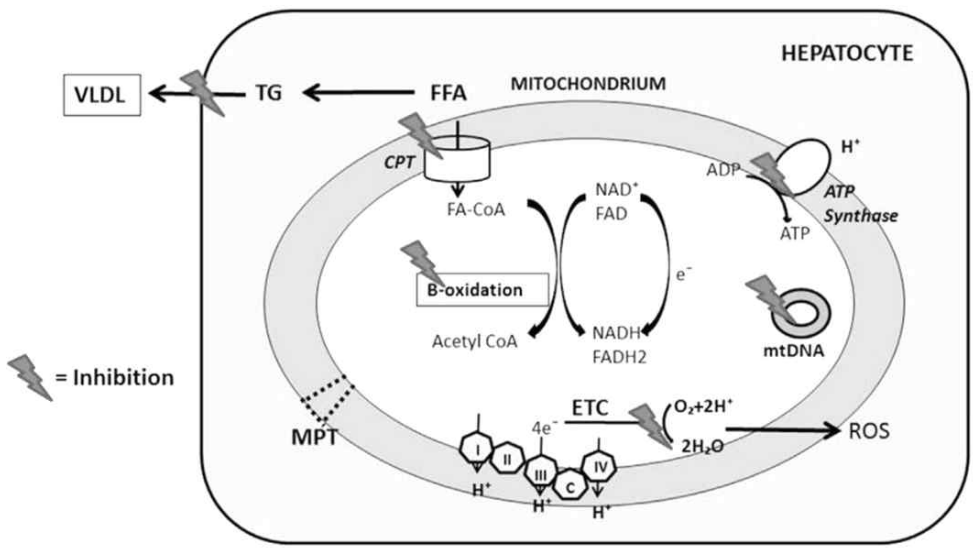

Figure 2. Mechanism of drug-induced hepatic steatosis (Patel *et al.,* 2013)

Inhibition of entry of long-chain fatty acids (FFA) via the carnitine palmitoyl shuttle (CPT) and inhibition of β-oxidation lead to increased free fatty acids, which are esterified into triglycerides. Transport of triglycerides (TG) as very low-density lipoprotein (VLDL) can be blocked by some drugs.

1.2. Autophagy

Autophagy is a highly conserved catabolic process that is involved in maintaining homeostasis under various conditions of cellular stress. It prevents cell damage, promotes survival in the event of energy or nutrient shortage, and responds to various cytotoxic insults. It serves as a regulator of protein homeostasis via the degradation and recycling of cellular components (Mizushima *et al.,* 2020)

In mammalian cells, there are three types of autophagy: macroautophagy, microautophagy, and chaperone-mediated autophagy (CMA). Macroautophagy is the major form of autophagy in which the cellular cargo is sequestered within a double-membraned vesicle, autophagosome. Microautophagy involves the direct engulfment of cytoplasmic contents by lysosomes. Little is known about the microautophagy in mammalian cells due to the limited number of its analysis tools. Chaperone-mediated autophagy (CMA) is a selective autophagy that involves the heat shock cognate protein (HSC70; also known as HSPA8) and lysosomal associated-membrane protein 2A (LAMP2A) protein. CMA selectively degrades a subset of cytosolic proteins. HSC70 brings the substrate proteins to the lysosomal surface and translocates them into the lysosome for degradation (Dikic *et al.,* 2018) (Figure 3).

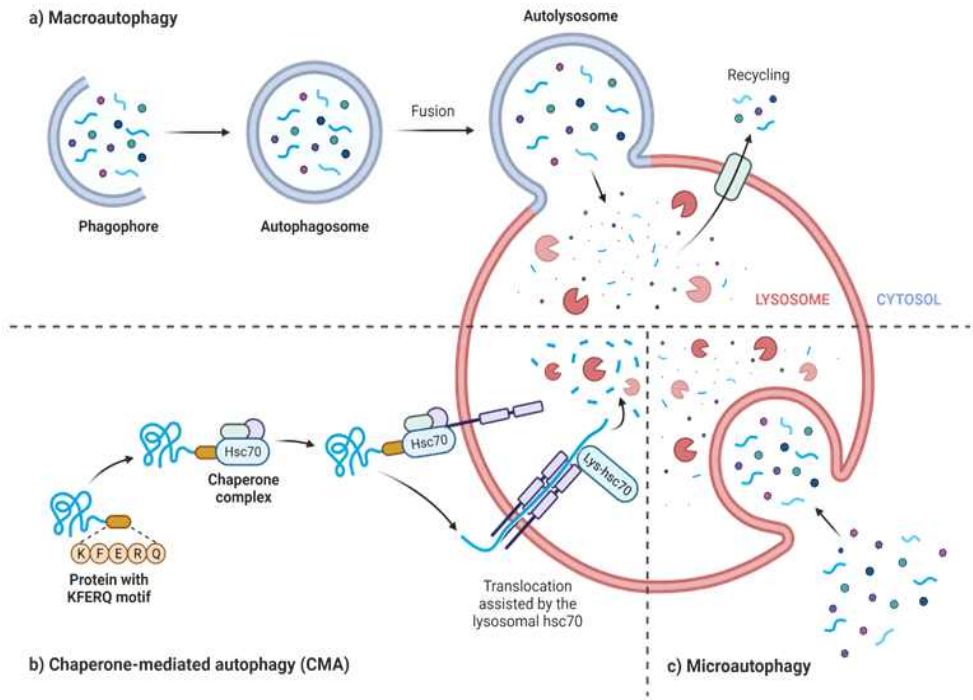

Figure 3. Three different types of autophagy

There are three primary types of autophagy: macroautophagy, microautophagy, and chaperone-mediated autophagy. Macroautophagy employs de novo formation of autophagosomes, transporting cargo to the lysosome. Chaperone-mediated autophagy selectively binds to cytosolic proteins and translocates proteins to the lysosome. Microautophagy involves the direct uptake of cargo through invagination of the lysosomal membrane.

1.3. Chaperone-mediated autophagy (CMA)

1.3.1. Mechanism of CMA

Chaperone-mediated autophagy (CMA) is an intracellular catabolic pathway that mediates the selective degradation of cytosolic proteins in lysosomes. It contributes to the maintenance of proteostasis and to the cellular adaptation to stress (Kaushik *et al.,* 2011). CMA only targets proteins with a motif recognized by the HSC70 chaperone. The substrate proteins for degradation via CMA contain a pentapeptide motif biochemically related to KFERQ, which is required for their targeting to the lysosome. The properties of the residues that constitute the motif, rather than the specific amino acids, determine whether the CMA-targeting chaperone HSC70 can bind to this region (Jackson *et al.,* 2016) (Figure 4).

During CMA, proteins are targeted by interacting with a cytosolic chaperone HSC70 that recognizes and binds to a pentapeptide KFERQ motif on the cargo protein. This interaction enables the cargo protein to transport to the lysosomal membrane protein called LAMP2A for its degradation. Multimerization of LAMP2A into a multimeric protein complex is essential for the translocation of the substrate into the lysosomal lumen (Kaushik *et al.,* 2018) (Figure 5).

Because of the broad spectrum of proteins that are susceptible to the degradation by CMA, the pathway has been involved in physiological and pathological processes such as lipid and carbohydrate metabolism, as well as neurodegenerative diseases.

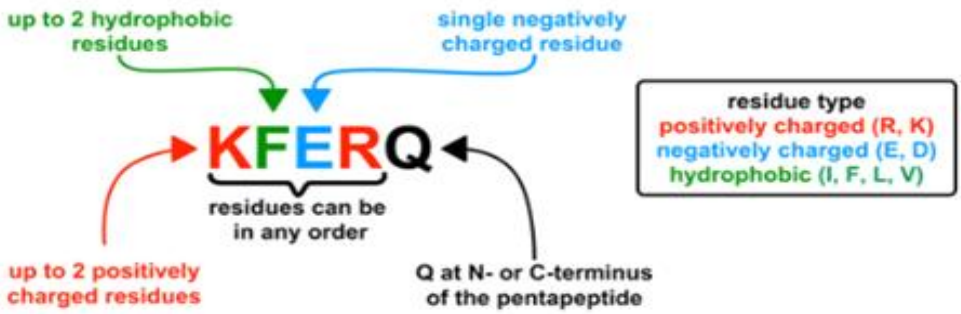

Figure 4. Proteins are recognized for CMA by KFERQ-like motif (Jackson *et al.,* 2016)

The CMA motif may contain up to two hydrophobic residues [isoleucine (I), phenylalanine (F), leucine (L) or valine (V)], up to two positive residues [arginine (R) or lysine (K)] and a single negatively charged residue [glutamate (E) or aspartate (D)] flanked at either the N-or C-terminus of the pentapeptide by a single glutamine (Q) residue. This is often referred to as a KFERQ or KFERQ-like motif

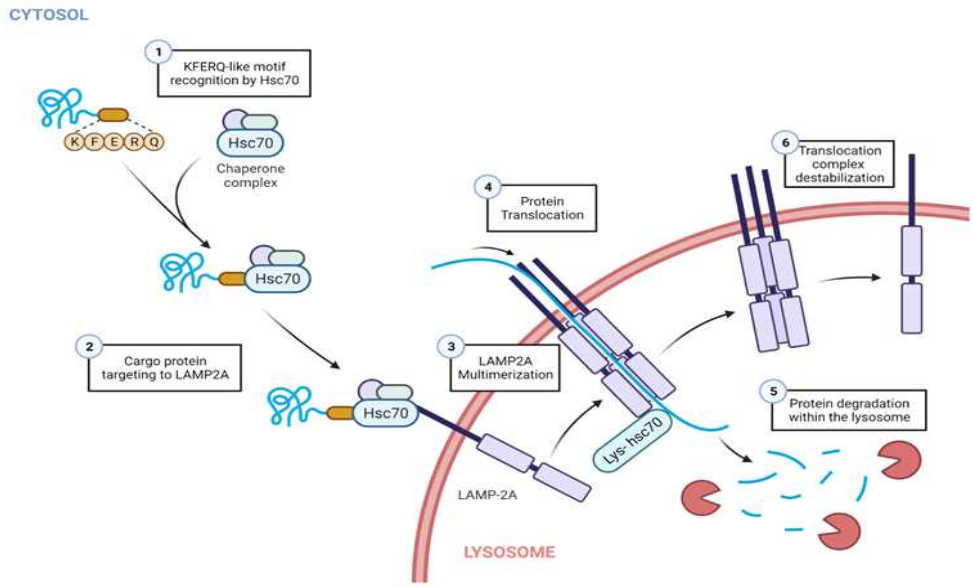

Figure 5. General scheme of chaperone-mediated autophagy (CMA) process (Modified from Kaushik *et al.,* 2018)

Proteins degraded through CMA are recognized by hsc70 in the cytosol and are targeted to the lysosomal membrane where they bind to LAMP2A. Substrate binding triggers multimerization of LAMP2A to form the complex that mediates substrate translocation.

1.3.2. CMA and hepatic steatosis

CMA has an important role in lipid homeostasis by regulating the lysosomal degradation of diverse proteins involved in lipid metabolism. It is reported that CMA inhibits lipid accumulation under lipid challenges. Lysosomal LAMP2A expression was reduced in the liver of mice exposed to cholesterol diet and high-fat diet. Dietary lipids reduced the stability of LAMP2A at the lysosomal membrane (Rodriguez-Navarro *et al.,* 2012). Evidence for the role of CMA in hepatic steatosis was obtained with the generation of liver-specific conditional knockout (KO) mouse for LAMP2A, the rate-limiting factor in CMA. LAMP2A KO mice showed enlarged and discolored livers, as well as elevated lipid levels. The proteomic analysis in lysosomes from the liver tissues of LAMP2A KO mice revealed that almost 30% of the hepatic proteins were CMA substrates that participate in lipid metabolism. Their degradation was decreased in LAMP2A KO mice, leading to profound hepatic steatosis. This finding supports the idea that loss of LAMP2A contributes to dysregulation of lipid metabolism and thereby aggravates fatty liver disease (Schneider *et al.*, 2014).

Taken together, blockage of hepatic CMA activity leads to alterations in hepatic lipid metabolism and the onset of fatty liver disease.

1.4. Regulation of lipid metabolism by CMA

1.4.1. Degradation of lipid droplet

Lipid droplets (LDs) are dynamic cytoplasmic organelles that play essential roles as lipid reservoirs and substrates for energy metabolism. LDs have a unique architecture consisting of a neutral lipid core enclosed by a phospholipid monolayer and a family of coat proteins such as perilipins (PLINs). The synthesis and degradation of LDs are controlled by diverse cellular signaling pathways necessary to maintain the energy and metabolic balance.

Catabolism of LDs into free fatty acid is a crucial pathway required to generate energy. Degradation of LDs occurs by two mechanisms: lipolysis or lipophagy. In lipolysis, protein kinase A phosphorylates PLIN1 proteins, leading to their proteasomal degradation and activation of adipose triglyceride lipase, which initiates triacylglycerols hydrolysis to generate diacylglycerols and free fatty acids (Souza *et al.,* 2002). Lipophagy is the autophagic pathway that plays a role in lipid degradation. In lipophagy, a small portion of LDs are selectively sequestered in autophagosomes and delivered to lysosomes for degradation (Dong *et al.,* 2011).

The pathological accumulation of lipids by defects in lipophagy or lipolysis has been linked to the development of metabolic disorders, including non-alcoholic fatty liver disease, coronary artery disease, and lysosomal storage diseases (Ward *et al.,* 2016).

1.4.2. Role of CMA in lipid droplet catabolism

A recent study demonstrated that the LD surface proteins, PLIN2 and PLIN3, are substrates of CMA (Kaushik *et al.,* 2015). Their degradation was reported to be an initial step that facilitates the degradation of the lipid component in the LD core by lipolysis or lipophagy (Ward *et al.,* 2016)

HSC70 binds to the KFERQ motif within PLIN proteins. CMA selectively degrades PLINs from the lipid droplet surfaces. Elimination of PLINs initiates the recruitment of cytosolic lipases to the lipid droplets, resulting in the degradation of lipid droplets. When CMA activity is compromised, however, PLINs surrounding lipid droplets are accumulated. The inability to remove PLINs from the surface of lipid droplets prevents access of cytosolic lipases to the lipid core and inhibits lipolysis. (Kaushik *et al.,* 2015) (Figure 6)

In addition, further studies demonstrated that phosphorylation of PLIN2 triggers its degradation by CMA. HSC70 interaction with PLIN2 promotes AMPK-mediated PLIN2 phosphorylation. Phosphorylation PLIN2 was released from lipid droplets and degraded by CMA. CMA-dependent removal of PLIN2 allows the arrival of cytosolic lipase to the lipid core, resulting in lipolysis. (Kaushik *et al.,* 2016)

In summary, selective degradation of PLIN2 by CMA and subsequent activation of lipolysis or lipophagy are critical cellular pathways of LD breakdown.

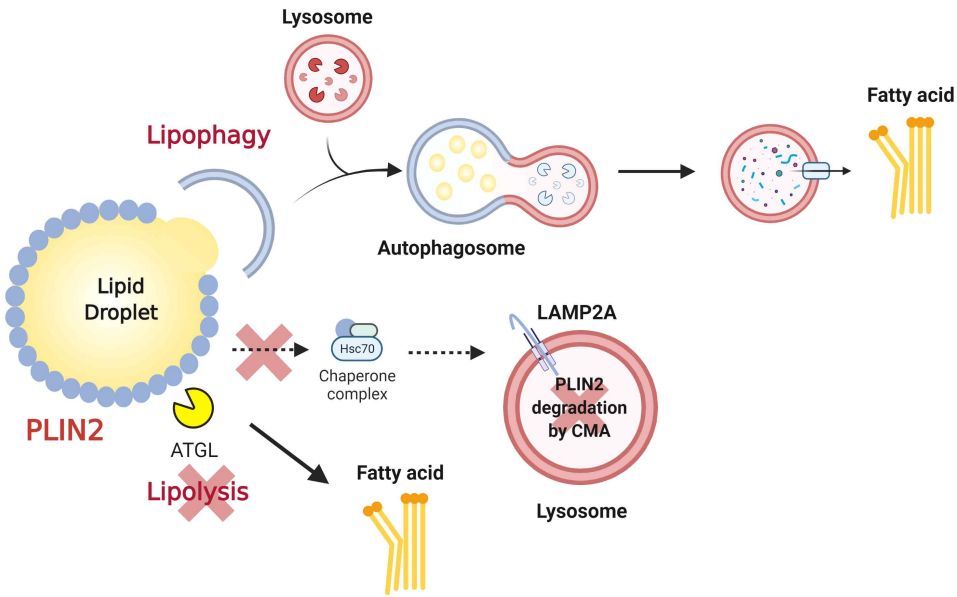

Figure 6. Regulation of lipid droplet catabolism by CMA (Modified from Kaushik *et al.,* 2015)

Lipid droplet (LD) catabolism in hepatocytes is mediated by a combination of lipolysis and a selective autophagic mechanism called lipophagy. When CMA is blocked, the degradation of lipid droplet-coating protein PLIN2 is inhibited and prevent access of lipases to the lipid core resulting in lipolysis inhibition.

1.5. Regulation of LAMP2A

LAMP2A is one of the three splice variants of a single gene, LAMP2. LAMP2A, LAMP2B, and LAMP2C have identical luminal regions but different transmembrane and cytosolic regions. LAMP2A is the only isoform required for CMA. Although LAMP2A is not the most abundant of the three isoforms, its blockage is known, to date, as the most specific way to inhibit CMA. (Bandyopadhyay *et al.,* 2008)

Because LAMP2A is the main regulator of CMA activity, five main pathways that regulate LAMP2A are reported to modulate CMA activity. Among them, the regulation of its expression, trafficking, and stabilization are key aspects of CMA activation (Figure 7).

(1) *De novo* LAMP2A synthesis: Nuclear factor of activated T cells 2 (NFATC2), also known as NFAT1, is recruited to the *Lamp2* promoter to induce LAMP2A expression, NFATC2 recruitment mediates the response to reactive oxygen species (ROS) in activated murine T cells (Valdor *et al.,* 2014). Together with NFATC2, nuclear factor erythroid 2-related factor 2 (NRF2) controls the basal and inducible expression of LAMP2A (Pajares *et al.,* 2018).

(2) LAMP2A trafficking to the lysosome

LAMP2A trafficking into the lysosomal membrane is inhibited by cystinosin, Rab11, and Rab-interacting lysosomal protein dysfunctions (Zhang e*t al.,* 2017).

(3) LAMP2A stability in the lysosomal membrane

Sorting nexin 10 (SNX10) facilitates the trafficking of cathepsin A (CTSA) into lysosomes, where it is processed into its active form.

Active CTSA interacts with and stimulates the degradation of LAMP2A on the lysosomal membrane (You *et al.,* 2018).

(4) The stability of LAMP2A translocation complex

Glial fibrillary acidic protein (GFAP) stabilizes LAMP2A multimeric translocation complex. GTP-mediated release of elongation factor 1α (EF1α) from the lysosomal membrane promotes self-association of GFAP, decreasing the stability of the complex and consequently inhibiting CMA (Bandyopadhyay *et al.,* 2010).

(5) Post-translational Regulation of HSC70

Histone deacetylase 6 (HDAC6) regulates HSP90 acetylation, thus controlling its interaction with LAMP2A and HSC70 (Su *et al.,* 2016).

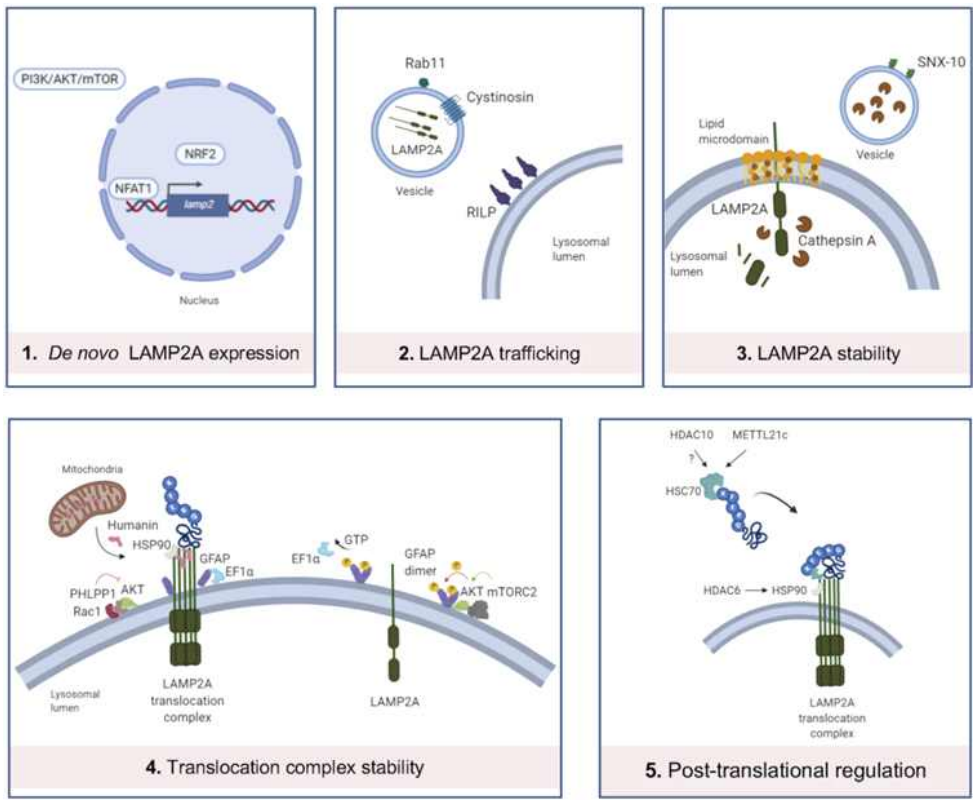

Figure 7. Regulation of LAMP2A

(Auzmendi-Iriarte *et al.*, 2021)

1.6. Sorting nexin 10 (SNX10) and Cathepsin A (CTSA)

Lysosomal Cathepsin A (CTSA) belongs to the serine protease cathepsin family. It is a multifunctional enzyme with a catalytic and protective function. In a recent study by Cuervo *et al.*, the protease activity of CTSA triggers the degradation of the LAMP2A protein. The activity of CMA can be regulated by the rate of assembly/disassembly of the LAMP2A multimeric complex. Mature CTSA in the lysosome binds to the lysosomal membrane and facilitates LAMP2A's cleavage from multimer to monomer (Cuervo *et al.,* 2003)

Sorting nexin 10 (SNX10) is one of the simplest structured isoforms in sorting nexin family. Sorting nexin family is evolutionarily conserved and involved in vesicular trafficking between cellular compartments. A recent study by You *et al.* demonstrated the role of SNX10 in alcohol-induced liver steatosis. They found that SNX10 deficiency alleviates alcoholic liver injury by activating CMA through upregulated transcription and stability of LAMP2A (You *et al.,* 2018) (Figure 8).

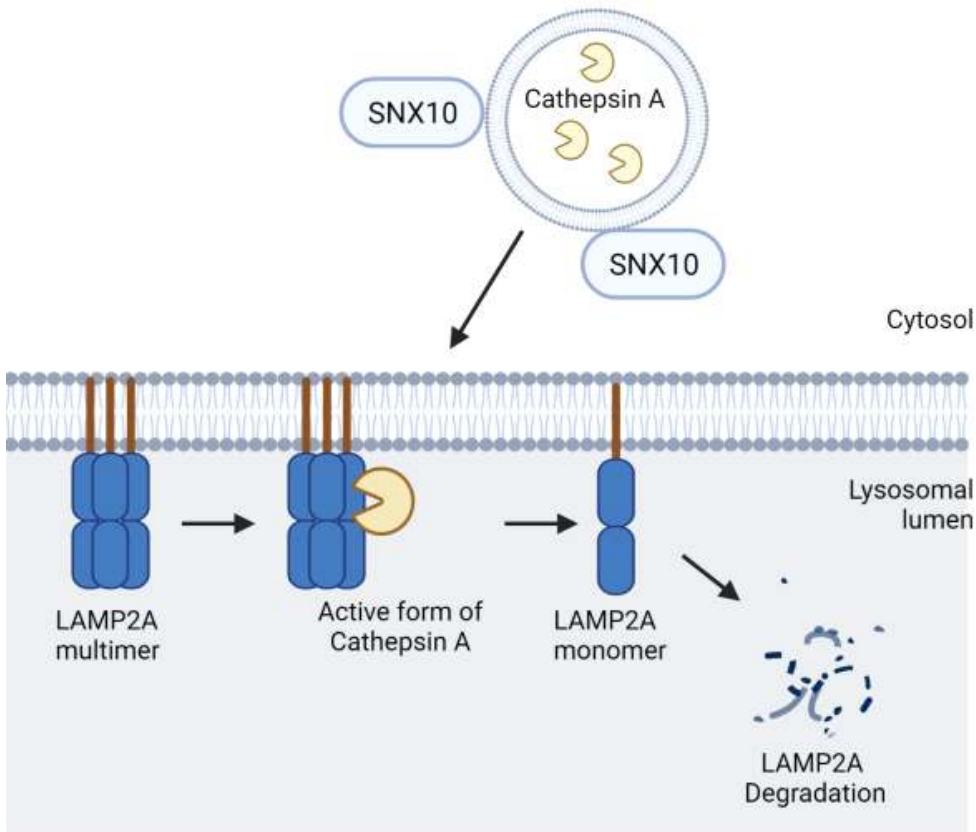

Figure 8. The role of SNX10 and CTSA in maintaining LAMP2A stability.

Sorting nexin 10 (SNX10) facilitates the trafficking of cathepsin A (CTSA) into lysosomes where it is processed into its active form. Active CTSA interacts with LAMP2A multimer and stimulates the degradation of LAMP2A multimer to monomer on the lysosomal membrane.

1.7. Endoplasmic reticulum stress

1.7.1. The UPR (Unfolded protein response) signaling pathway

The endoplasmic reticulum (ER) stress occurs when the ER protein folding capacity is overwhelmed. It is characterized by misfolded proteins accumulated in the ER lumen. In response to ER stress, cells have evolved a conserved signal transduction pathway, collectively termed the unfolded protein response (UPR). A critical step in UPR signaling is the initial detection of ER stress, the process by which unfolded and misfolded proteins are recognized by UPR, leading to activation and downstream signaling. (Lin *et al.,* 2008)

Three key transmembrane sensors control the UPR signaling pathway: activating transcription factor 6α/β (ATF6), PKR-like ER kinase (PERK), and inositol requiring enzyme 1α/β (IRE1). (Corazzari *et al.,* 2017)

(1) ATF6 becomes an active transcription factor when it is translocated to the Golgi apparatus and cleaved by proteases. Activated ATF6 stimulates the expression of ER chaperones.

(2) PERK decreases protein translation by phosphorylating eukaryotic translation initiation factor 2α (eIF2α). Phosphorylated eIF2α enhances transcription of ATF4 and subsequently increases transcription of the cytoprotective gene. In addition, phosphorylated eIF2α induces apoptosis through upregulation of C/EBP-homologous protein (CHOP).

(3) IRE1 phosphorylation stimulates endoribonuclease activity and splices X-box-binding protein 1 (XBP1) mRNA to form a potent transcriptional activator, XBP1s (a spliced form of XBP1).

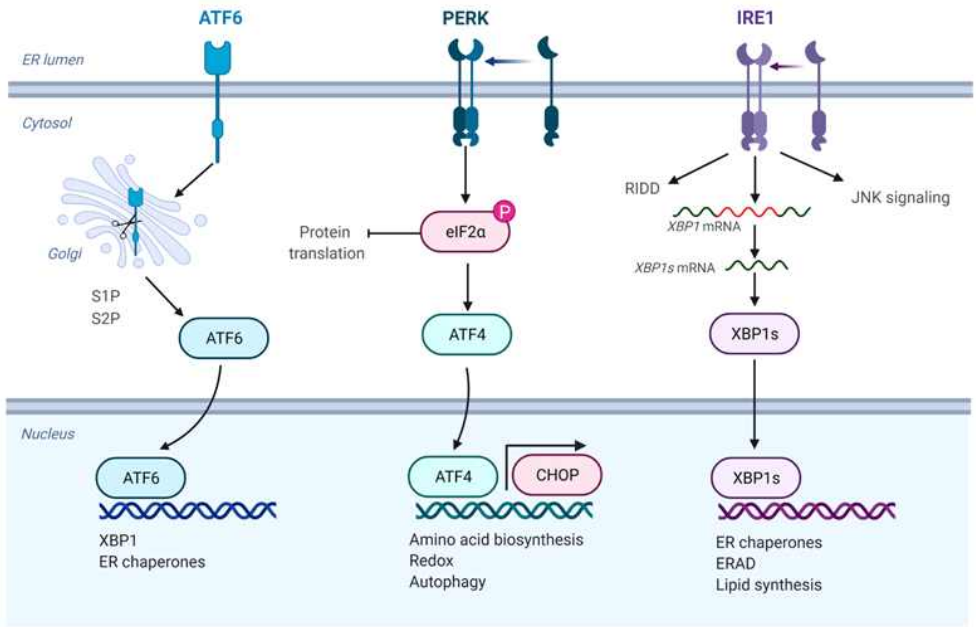

Figure 9. Overview of the UPR (Unfolded protein response) signaling pathway (Modified from Li *et al.,* 2020)

Upon induction of ER stress, the ER chaperone BiP binds to unfolded proteins and dissociates from three ER stress sensors, namely PERK, ATF6 and IRE1.

1.7.2. ER stress involved in NSAID-induced toxicity

As previously mentioned, the use of NSAIDs is commonly associated with gastrointestinal adverse events, partially because of their acidic characteristics and the inhibition of cyclooxygenase (COX).

However, recent studies revealed that NSAIDs also induce ER stress, which is an upstream mechanism responsible for apoptosis. Exposure of cells to indomethacin, diclofenac, or ibuprofen, a commonly used NSAID, induced GRP78 as well as CHOP, a transcription factor involved in apoptosis. Moreover, the indomethacin-induced apoptosis was suppressed by the expression of the dominant-negative form of CHOP. These findings provide evidence on the contribution of ER stress to NSAID-induced apoptosis (Tsutsumi *et al.,* 2004).

In addition, it is reported that the ER stress response is involved in NSAID-induced hepatotoxicity. In a rat hepatocyte, various NSAIDs induced CHOP expression (Nadanaciva *et al.,* 2013). In a Huh7 hepatoma cell line, the treatment of diclofenac or indomethacin triggered the activation of the UPR response (Franceschelli *et al.,* 2011). Another study showed that CHOP KO mice were shown to be protective from necrosis-mediated hepatotoxicity followed by acetaminophen gavage (Uzi *et al.,* 2013). Based on these previous findings in the literature, it was estimated that ER stress mediates NSAID-induced hepatotoxicity.

1.8. The aim of study

The goal of this study is to identify the effect of NSAIDs on CMA and the role of ER stress in NSAID-induced hepatic lipid accumulation.

First, I assessed the effect of several NSAIDs on hepatic lipid accumulation *in vitro* and *in vivo*.

Second, I studied the inhibitory effect of NSAIDs on CMA activity. I hypothesized that CMA inhibition by NSAIDs suppressed the degradation of CMA substrates, including PLIN2. Indeed, CMA reactivation reversed diclofenac-induced lipid accumulation in mouse primary hepatocytes.

Third, I investigated the mechanism by which NSAIDs decrease CMA activity. Exposure to NSAID increased the expression of SNX10 and activation of CTSA, thereby inhibiting CMA activity.

Fourth, this study delineated the cause of the upregulation of SNX10 expression. NSAID induced ER stress that increased SNX10 expression level, resulting in the CMA inhibition and hepatic lipid accumulation.

2. Materials and Methods

2.1. Cell culture

2.1.1. Isolation of mouse primary hepatocytes

Mouse primary hepatocytes (MPH) were isolated from the livers of 8 to 10 weeks old specific pathogen-free male C57BL/6 mouse (25g) by perfusion of the liver using collagenase type Ⅳ. Mice were anesthetized and abdominal cavity were open. Inferior vena cana was cannulated with 24G catheter and portal vein was cut for drainage. The livers were flowed with pre-warmed HBSS (Hanks' balanced salt solution; Gibco, 14170112) containing 0.5mM EDTA and 25mM HEPES to remove blood. And then, HBSS with 5mM $CaCl_2$ and 0.2mg/ml of Collagenase type IV was perfused to the liver for hepatocyte isolation. After digestion, the liver was excised, put into Williams' medium E (WME; Sigma, W4128) containing 10% fetal bovine serum (FBS; Gibco, 16000044), 1% antibiotic-antimycotics (A/A; Gibco, 15250062), 0.2μg/ml of dexamethasone (Sigma) and 0.6μg/ml of insulin (Sigma). Medium was filtered through 100 micron mesh and centrifuged at 500 rpm for 3 minutes. Cell pellet was resuspended with medium, and the viability was measured by trypan blue and produced nearly 90% homogenous viable hepatocytes. Hepatocytes were seeded at collagen-coated plate. Cells were stabilized for overnight, and then incubated in WME with 10% FBS, 1% antibiotic-antimycotics.

2.1.2. Cell line culture

HepG2 and AML12 cells were obtained from the American Type Culture Collection (ATCC) and SN4741 was kindly gifted from Dr. Yong-Keun Jung (Seoul National University, Korea). HepG2 cells and SN4741 cells were maintained in Dulbecco's modified Eagle's medium (DMEM; hyclone, SH.30021.01) supplemented with 10% FBS and 1% A/A. AML12 cells were maintained in DMEM/F12 (Gibco, 11320-033) with 0.5 μg/ml of insulin (Sigma), 0.5 μg/ml transferrin, 5 ng/ml selenium (ITS; Gibco, 41400045), and 40 ng/ml dexamethasone containing 10% FBS, 1% A/A. HepG2 and AML12 cells were incubated at 37 °C, and SN4741 cells were incubated at 33 °C in humidified air containing 5% CO2 incubator.

2.2. Nile Red Assay

Intracellular lipid accumulation was quantified using Nile Red, a fluorescent dye that binds to neutral lipids. HepG2 cells and AML12 cells were seeded in 96 well black plates at a density of $8*10^4$ cells per well and incubated with chemicals for 24 hr. On the following day, cells were fixed with 4% paraformaldehyde containing DAPI for 10 minutes and stained with 1 μg/ml Nile Red solution for 10 minutes, and washed with phosphate-buffered saline (PBS). Fluorescence was measured using a microplate fluorescence reader (Molecular Devices) at excitation and emission wavelengths of 488nm and 580nm, respectively. Data were normalized by DAPI determined at the excitation and emission wavelengths of 365nm and 488nm,

respectively.

2.3. Triglyceride analysis

Total lipids were extracted from liver homogenates prepared from 100 mg of mouse livers and mouse primary hepatocytes using chloroform/methanol mixture (2:1. v/v). Triglyceride concentration was determined enzymatically using a commercially available enzymatic kit (Sigma, TR0100) following the manufacturers' protocol.

2.4. Animal experiments

SPF Male C57BL/6 mice (aged 7 weeks) were purchased from Jackson Laboratory via Orient Bio and allowed to acclimate for 1 week at air-conditioned room (24℃) with a 12 hr light/dark cycle, and allowed to free access to water and food for 1 week. After adaption period, the animals were randomly divided into the following 4 groups (6 mice per group). (1) The vehicle group was received intraperitoneally with 0.5% DMSO in saline. (2) Diclofenac group was administered diclofenac (100 mg/kg) intraperitoneally twice every 12 hr. (3) AR7 group was administered AR7 (10 mg/kg) intraperitoneally twice every 12 hr. (4) Diclofenac/AR7 group was administered AR7 (10 mg/kg) intraperitoneally twice 1 hr before diclofenac administration. Next day, mice were anesthetized with Zoletil 50 (Virbac) and sacrificed. All animal experiments were carried out in accordance with animal experiment guidelines with the approval of the Institutional Animal Care and Use Committee of Seoul National

University.
(approval number: SNU-200615-2-1)

2.5. Serum biochemistry

Whole Blood samples collected through cardiac puncture were centrifuged at 3000 rpm for 10 minutes. Serum supernatants were aliquoted and kept at -80℃ for further use. Serum levels of alanine aminotransferase (ALT), aspartate aminotransferase (AST), Triglyceride (TG) were measured using an Automated Chemistry Analyzer (Prestige 24I; Tokyo Boeki Medical System, Tokyo, Japan) according to the manufacturer's protocol.

2.6. Histological analysis

The liver tissues were fixed in 4% paraformaldehyde and embedded in paraffin blocks. Parrafin blocks were cut into 5 μm sections and stained with hematoxylin and eosin (H&E). For Oil Red O staining, frozen liver tissues were cut into 7-mm sections and mounted to microscope slides.

2.7. Immunoblot analysis

Liver tissue was homogenized in 3-fold volume of 0.15M KCl (USB, Cleveland, OH). Cells and mouse liver tissue homogenates were washed with PBS and lysed in buffer containing 50 mM HEPES (Sigma, H4034), 150 mM NaCl (Sigma, S9888), 5 mM ethylene

glycol-bis(2-aminoethylether) -N,N,N',N'-tetraacetic acid (EGTA; Sigma, E0396), 50 mM β-glycerophosphate disodium salt (Sigma, G9422), 1% Triton-X 100 (Sigma, X100) and protease inhibitor cocktail (Roche, 11697498001). The lysates were then centrifuged at 14,000 rpm for 15 minutes. The supernatant was quantified by lowry assay. 25-35 ug of lysates were separated by SDS-polyacrylamide gel electrophoresis and then transferred to PVDF membrane (Merck Millipore, IPVH0001). Transferred proteins were blocked in 5% skim milk or bovine serum albumin probed with specific antibodies. Bound primary antibodies were detected using secondary antibodies against rabbit or mouse IgG and developed by Amersham ECL prime western blotting detection reagent (GE healthcare, RPN2232).

2.8. RNA preparation and qRT-PCR analysis

mRNA was extracted with the Easy-Blue Total RNA Extraction Kit (iNtRON, 17091). After extraction, complementary DNA (cDNA) was synthesized using QuantiTect Reverse Transcription Kit (QIAGEN, 205313). cDNA was amplified by qRT-PCR using iTaq Universal SYBR Green Supermix kit (Bio-Rad, 1725121) with a Stepone™ Real-Time PCR system (Applied Biosystems). The sequences of primers used for qRT-PCR are listed in Table 2.

2.9. Transient transfection

For RNAi transfection, HepG2 and mouse primary hepatocytes were seeded in 6 well plates 1 day before the transfection. The siRNA

duplexes targeting mouse Cathepsin A (Bioneer), human CHOP (Bioneer), mouse SNX10 (Santacruz) or control siRNA were transfected using Lipofectamine RNAiMAX (Invitrogen, 13778075) according to the manufacturer's protocol.

For gene overexpression, mouse LAMP2A (Origene, RC221216) and human CHOP (Origene, RC201301) overexpression vector were transfected using Lipofectamine 2000 (Invitrogen, 11668027).

2.10. Confocal microscopy

2.10.1. BODIPY 493/503 staining

Cells were grown on coverslips and fixed with 4% paraformaldehyde in PBS for 10 minutes. For BODIPY staining, cells were loaded with 10 μg/ml BODIPY 493/503 in PBS for 20 minutes. The nuclei were stained with DAPI. The cells were washed three times with PBS and coverslips were mounted using ProLong Gold Antifade Reagent (Life Technologies, P36930) and images were captured with TCS SP8 confocal laser scanning microscope (Leica Microsystems). 5 images were randomly selected and quantified using Image J software.

2.10.2. Immunofluorescence analysis

For immunofluorescence microscopy, cells were rinsed with PBS and fixed with 4% paraformaldehyde in PBS for 10 minutes. For visualization, fixed cells were subjected to a blocking solution (PBS

containing 1% normal horse serum) and permeabilized in 0.1% Triton X-100. Cells were incubated with appropriate primary antibodies (1:200 dilution in blocking solution) at 4℃ overnight. Next day, The cells were washed three times with PBS and incubated with secondary Alexa-Flour 488, 596 dye-labeled antibodies (1:1000 in blocking solution, Thermo Fisher Scientific). The nuclei were stained with DAPI. Coverslips were mounted using ProLong Gold Antifade Reagent (Life Technologies, P36930) and images were captured with TCS SP8 confocal laser scanning microscope (Leica Microsystems). 5 images were randomly selected and quantified using Image J software.

2.10.3. Measurement of CMA activity using PA-mCherry- KFERQ reporter plasmid

pSIN-PAmCherry-KFERQ-NE was obtained from Addgene (plasmid # 102365). HepG2 cells seeded in 12-well plates with microscope cover glasses were infected with pSIN-PAmCherry-KFERQ-NE lentiviral particle. Cells were photoactivated with a 405 nm light-emitting diode LED for 5 min with the intensity of 3.5 mA. After 16 hr, cells were fixed with 4% paraformaldehyde and analyzed using confocal microscopy. Quantification was performed by counting the red puncta.

2.11. Lysosomal fractionation

Cells and 100 mg of liver tissues were homogenized in the cold room with a glass Teflon homogenizer. Lysosomal fractions were prepared using ultracentrifuge at 141,000 rpm for 2 hr and lysosome enrichment kit (Thermo Fisher Scientific, 89839) and according to the manufacturer's protocol.

2.12. Measurement of intracellular Ca^{2+} levels

HepG2 cells were seeded in 48 well plates and incubated overnight. On the following day, cells were treated with NSAIDs and were incubated with 2 μM Fluo-3 AM (Thermo Fisher Scientific, F1241) for 30 minutes. After treatment, cells were observed using Cytation 3 (BioTek). Green fluorescence values were determined using Cytation 3 program.

2.13. Antibodies and reagents

Antibodies against Bip (3183), CHOP (2895), COX2 (12282), GAPDH (2118), LC3B (2775) and PK (7067) were purchased from Cell Signaling Technology. Antibodies against PLIN2 (NB110-40877) and SNX10 (NBP1-79562) were purchased from Novus Biologicals. Antibodies against LAMP2A (ab18528) and COX1 (ab109025) were purchased from Abcam. The antibodies against β-actin (Santa Cruz Biotechnology; sc-47778), CTSA (Origene; TA332731) and LAMP1 (Developmental Studies Hybridoma Bank; 1D4B) were obtained as indicated. BODIPY493/503 (D3922) and DAPI solution (62248) were purchased from Thermo Fisher Scientific. BAPTA-AM (A1076),

diclofenac sodium (D6899), Mito-Tempo (SML0737), oleate (O1008), leupeptin (L2884), rapamycin (553210), clioquinol (ClioQ; 233165), Nile Red (72485), 4-phenylbutyrate (SML0309), taurodeoxycholic acid sodium salt (T0266) and tunicamycin (T7765) were from Sigma Aldrich.

2.14. Statistical Analysis

The statistical analysis of the data was performed using GraphPad Prism 7 (GraphPad Software, San Diego, CA, USA). Experimental data were presented as mean ± S.D. *in vivo* and *in vitro* experiments. Data were subjected to student's t-test or one-way ANOVA analysis followed by Turkey's multiple comparison test. P values < 0.05 were considered statistically significant.

Table 2. Sequences of qRT-PCR primers used in the study

Species	Gene	Forward Primer (5′ to 3′)	Reverse Primer (5′ to 3′)
Human	*GAPDH*	AACGGATTTGGTCGTATT	GCTCCTGGAAGATGGTGA
Human	*PLIN2*	GTAGAGTGGAAAAGGAGCAT	CAGTCAGCTGAGGATAAAAGG
Human	*LAMP2A*	CTCTGCGGGGTCATGGTG	CGCACAGCTCCCAGGACT
Human	*ACTB*	AGGCACCAGGGCGTGAT	GCCCACATAGGAATCCTTCTGAC
Mouse	*Gapdh*	CGGTGCTGAGTATGTCGT	CTTCTGGGTGGCAGTGAT
Mouse	*Plin2*	CAGCCAACGTCCGAGATTG	CACATCCTTCGCCCCAGTT
Mouse	*Lamp2a*	AGGTGCTTTCTTGTCTAGAGCGT	AGAATAAGTAGTACTCCTCCCAGAGCTGC
Mouse	*Snx10*	GGGTTCGCTCTTAGGCGCTCG	GGACACGATCAACACGCGGTTCT
Mouse	*Actb*	CTGTCCCTGTATGCCTCTG	ATGTCACGCACGATTTCC

3. Results

3.1. NSAIDs induced hepatic lipid accumulation *in vitro* and *in vivo*

3.1.1. Several NSAIDs increased intracellular lipid levels *in vitro* and *in vivo*

To determine whether NSAIDs induce neutral lipid accumulation in hepatocytes, 7 NSAIDs were selected, 4 from acetic acid derivatives and 3 from propionic acid derivatives. To exclude artifacts from the drugs' differing cytotoxicity, the highest concentration was set in all cases to half of the IC_{50} determined by an MTT assay (data not shown). All of the tested NSAIDs increased the intensity of Nile Red fluorescence in HepG2 cells in a concentration-dependent manner. Diclofenac is a representative hepatotoxic drug of NSAIDs, and diclofenac is also a potent drug inducing lipid accumulation. Therefore, diclofenac was selected as the model compound to investigate the mechanism of hepatic lipid accumulation. Diclofenac-induced lipid accumulation was confirmed in mouse primary hepatocytes (MPH) and AML12 cells by increased Nile Red fluorescence. Diclofenac increased intracellular triglyceride levels in HepG2 cells and MPH. (Figure 10)

To confirm the effects of diclofenac *in vivo*, C57BL/6 mice were treated with diclofenac (100mg/kg) through intraperitoneal injection. Oil Red O staining and hepatic triglyceride levels revealed that diclofenac caused fatty liver *in vivo*. (Figure 11)

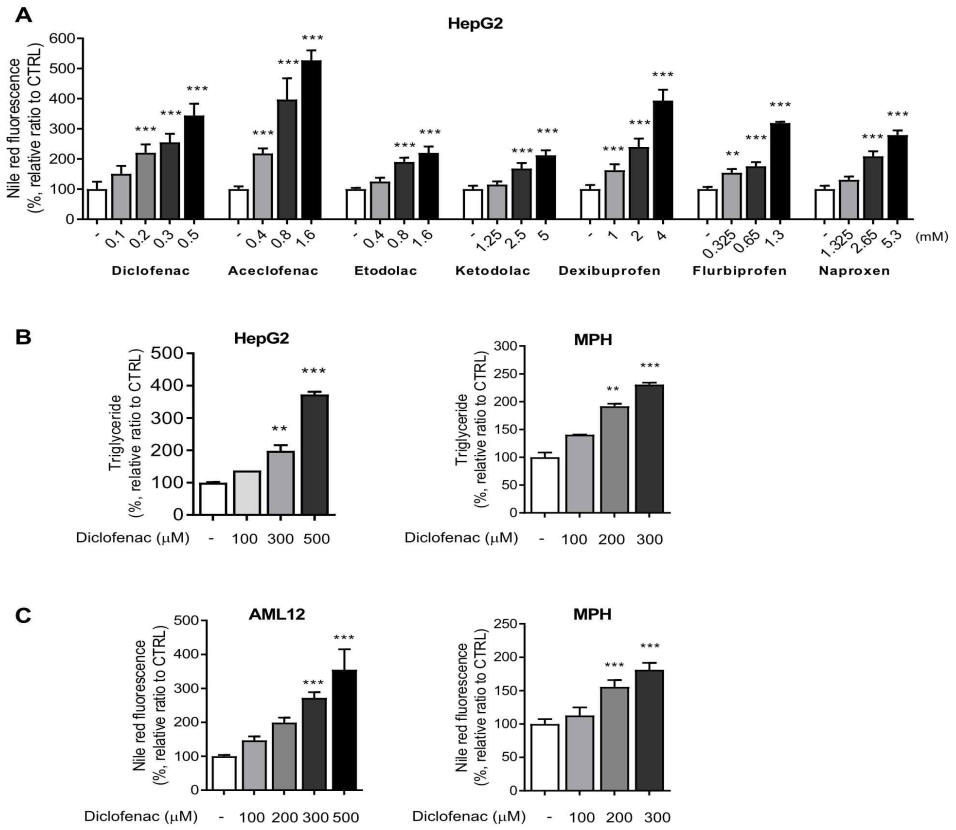

Figure 10. Several NSAIDs increased intracellular lipid levels *in vitro*
(A) HepG2 cells were treated with NSAIDs for 24 h, and intracellular neutral lipid levels were quantified using Nile-red dye; the excitation and emission wavelengths were 486 and 528 nm, respectively. (B) HepG2 cells and MPH were treated with diclofenac at the indicated concentration for 24 h, and intracellular triglyceride (TG) concentrations were quantified using an enzymatic kit. (C) AML12 and MPH were treated with diclofenac at the indicated concentration for 24 h, and intracellular neutral lipid levels were quantified using Nile-red dye; the excitation and emission wavelengths were 486 and 528 nm, respectively. Data are presented as mean ± SD of at least 3 independent experiments, as analyzed by one-way ANOVA followed by Tuckey's test. **$p < 0.01$, and ***$p < 0.001$, relative to the control group.

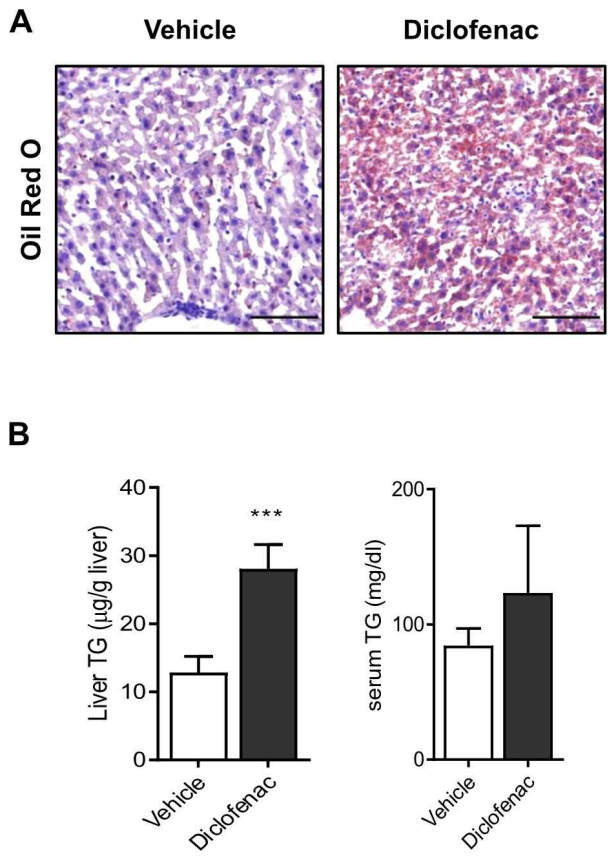

Figure 11. Diclofenac induced hepatic lipid accumulation *in vivo*

(A, B) C57BL/6 mice were intraperitoneally injected with diclofenac (100 mg/kg) and sacrificed after 24 h (n = 6). (A) Representative Oil Red O-stained liver sections demonstrating neutral lipids in the liver (Scale bars: 100 μm). (B) Liver TG and serum TG concentrations in the liver of mice were quantified using the enzymatic kit. Data are presented as mean ± SD of six *in vivo* experiments, as analyzed by student's t-test. ***$p < 0.001$.

3.1.2. Diclofenac induced hepatic lipid accumulation independent of lipogenic stimulus

To determine whether the diclofenac-induced lipid accumulation was associated with lipogenesis, MPH were treated with diclofenac and oleate, lipogenic stimulus, and changes in lipid droplets were detected by imaging analysis using BODIPY 493/503 dye. MPH accumulated more and larger LDs visible with BODIPY 493/503 under both the basal and oleate-treated conditions. The lipid-accumulating effects of diclofenac and oleate were synergistic. To further investigate whether diclofenac affects the lipogenesis pathway, the expression of genes associated with the lipogenesis pathway was explored. Treatment with diclofenac did not change the expression of lipogenic genes in protein levels and mRNA levels. These results provided that diclofenac did not affect the lipogenesis pathway. (Figure 12)

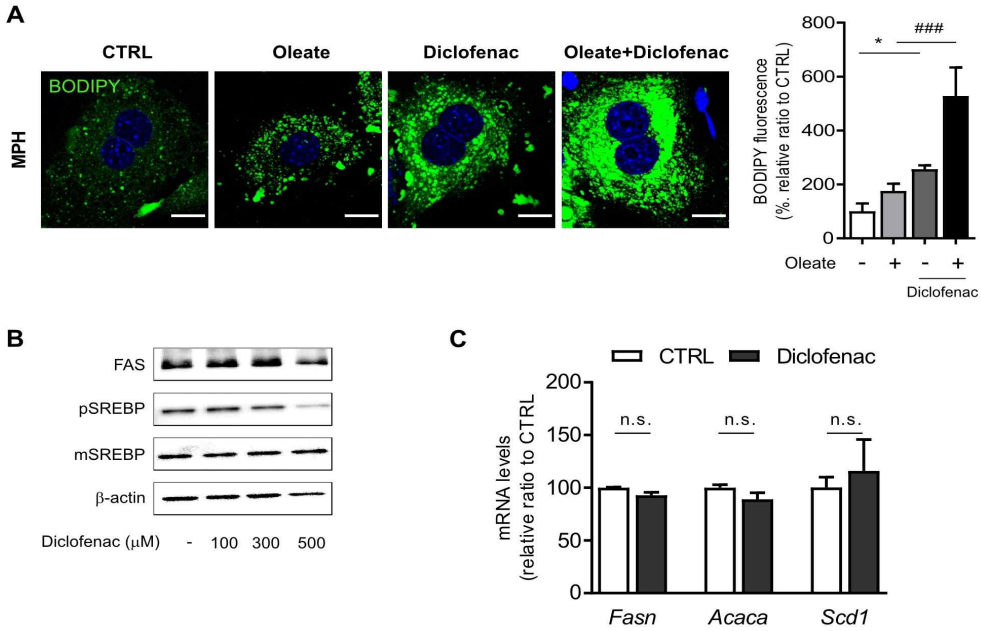

Figure 12. Diclofenac induced hepatic lipid accumulation independent of lipogenic stimulus

(A) MPH were treated with diclofenac (300 μM) and/or oleate (100 μM) followed by staining with BODIPY 493/503 (green). Nuclei were stained with DAPI (blue). Representative fluorescent images and quantitative data are shown (Scale bars: 20 μm). (B) MPH were treated with diclofenac at the indicated concentration for 24h, and the levels of FAS, pSREBP and mSREBP were analyzed by western blotting. (C) mRNA was extracted from MPH treated with diclofenac (300 μM) for 24 h, and mRNA levels of *Fasn, Acaca, Scd1* were analyzed by qRT-PCR Data are presented as mean ± SD of at least 3 independent experiments, as analyzed by one-way ANOVA followed by Tuckey's test. *$p < 0.05$, relative to the control group. ###$p < 0.01$, relative to the oleate-treated group. n.s.; non-significant relative to the control group.

3.2. NSAIDs increased the expression of CMA substrates in hepatocytes

3.2.1. Several NSAIDs induced the increase of expression of CMA substrates, PLIN2 and GAPDH.

LDs are surrounded by structural proteins of the perilipin (PLIN) family, and lipolysis requires the removal of these perilipins from lipid droplets (Sztalryda *et al.* 2017). A recent study has revealed that PLIN2 is one of the representative CMA substrate proteins associated with lipid metabolism (Kaushik *et al.* 2015). To identify whether the effect of NSAIDs on lipid accumulation is associated with CMA activity, NSAIDs treated *in vitro* model was used, and the expression of CMA substrate was monitored by western blot analysis. When HepG2 cells were treated with various NSAIDs, a dose-dependent increase was found not only in PLIN2 but in GAPDH, well-known CMA substrates. These results indicated that NSAIDs regulate the abundance of CMA substrates in hepatocytes, suggesting the possibility of CMA inhibition by NSAIDs. (Figure 13)

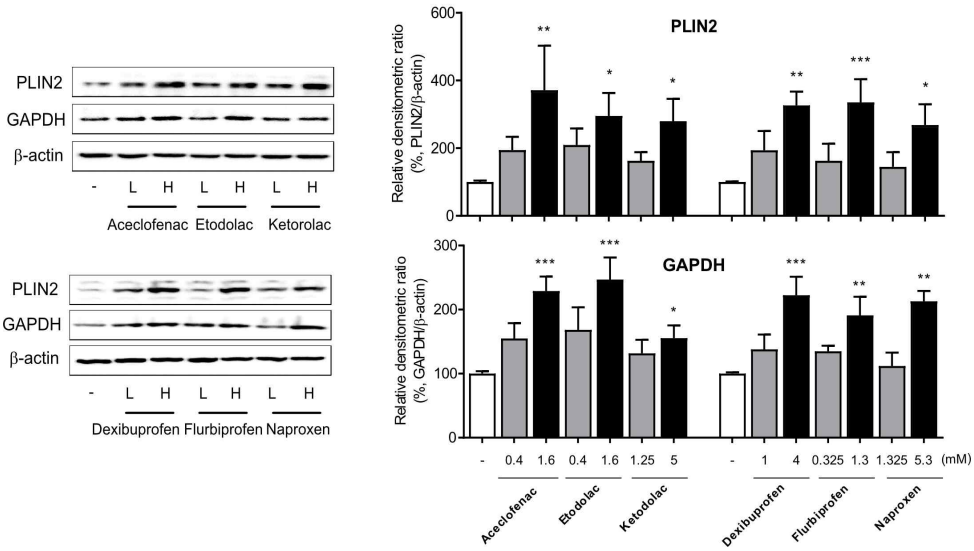

Figure 13. Several NSAIDs induced the increase of CMA substrates, PLIN2 and GAPDH

HepG2 cells were treated with the indicated concentration of NSAIDs for 24 h, and the levels of PLIN2 and GAPDH were analyzed by western blotting (L; Low concentration, H; High concentration). The right panel shows the densitometric quantification of the PLIN2 and GAPDH levels. Data are presented as mean ± SD of at least 3 independent experiments, as analyzed by student's t-test. *$p < 0.05$, **$p < 0.01$, and ***$p < 0.001$, relative to the control group.

3.2.2. Diclofenac increased the abundance of CMA substrate proteins *in vitro* and *in vivo*.

To confirm the effect of diclofenac on CMA substrates accumulation, the level of CMA substrate was evaluated in MPH. First, not only PLIN2 but also GAPDH were increased in a dose-dependent manner in MPH. To further investigate whether the increase in proteins of PLIN2 and GAPDH can be related to transcriptional changes, mRNA levels of *Plin2* and *Gapdh* were measured using qRT-PCR. However, diclofenac treatment did not change the mRNA levels of PLIN2 and GAPDH in MPH. Fluorescence microscopy analysis demonstrated that diclofenac increased the mean staining intensity of PLIN2 and enlarged the size of PLIN2-surrounded LDs. Next, the level of PLIN2 level was determined whether increased PLIN2 by diclofenac is related to the oleate-mediated lipogenic stimulus or not. The increase of PLIN2 by diclofenac was also observed under the lipogenic stimulus condition induced by oleate.

To confirm the effect of diclofenac in mice, mice were treated with 100mg/kg of diclofenac. Treatment with diclofenac significantly increased two CMA substrates, PLIN2 and GAPDH. These results indicate that CMA substrates are accumulated by diclofenac, which suggests the possibility of CMA inhibition by NSAIDs. (Figure 14)

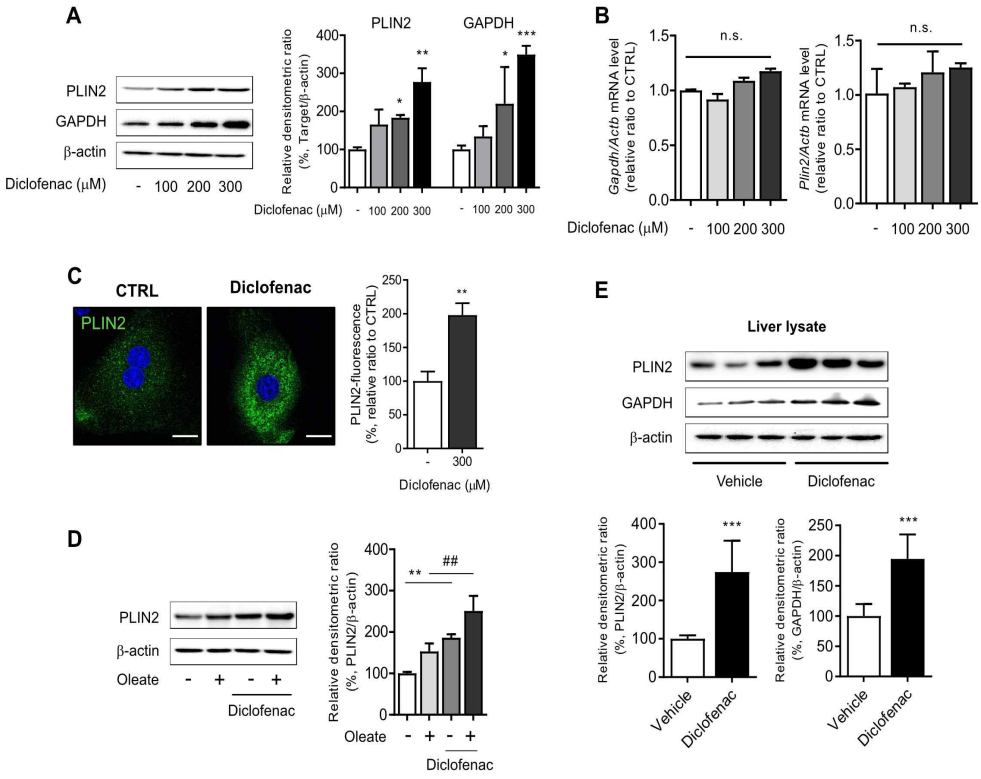

Figure 14. Diclofenac increased the abundance of CMA substrate proteins *in vitro* and *in vivo*.

(A) Western blot analysis of PLIN2 and GAPDH in MPH, treated with the indicated concentrations of diclofenac for 24 h. The right panel shows the densitometric quantification of the PLIN2 and GAPDH levels. (B) mRNA levels of *Gapdh* and Plin2 from MPH treated with the indicated concentrations of diclofenac for 24 h were analyzed by qRT-PCR. (C) MPH were treated with diclofenac (300 μM) for 24 h, and PLIN2 expression was determined by immunofluorescence staining, PLIN2 (green), DAPI (blue).

Representative fluorescent images of the cells are shown, and quantitative data are shown in the right panels (Scale bars: 20 μm). (D) MPH were treated with diclofenac (300 μM) and/or oleate (100 μM), and the levels of PLIN2 were analyzed by western blotting. (E) Proteins were extracted from the livers of mice administered with vehicle or diclofenac (100 mg/kg), and the levels of PLIN2 and GAPDH were analyzed by western blotting (n = 6). Data are presented as mean ± SD of at least 3 independent experiments, as analyzed by one-way ANOVA followed by Tuckey's test. *$p < 0.05$, **$p < 0.01$, and ***$p < 0.001$, relative to the control group. ##$p < 0.01$, relative to the oleate-treated group. n.s.; non-significant relative to the control group.

3.3 NSAIDs inhibited CMA by reducing the level of LAMP2A in the lysosome

3.3.1. Several NSAIDs including diclofenac decreased the protein level of LAMP2A.

CMA is a selective form of autophagy targeting only proteins with a motif recognized by the HSC70 chaperone. Lysosome-associated membrane protein type 2A (LAMP2A) is responsible for substrate binding and internalization to lysosomes, and thus, the lysosomal expression level of LAMP2A is a rate-limiting factor for CMA. Therefore, several NSAIDs were treated in HepG2 cells, and the expression of LAMP2A was measured using western blot analysis. All NSAIDs decreased the expression of LAMP2A in a concentration-dependent manner in HepG2 cells. Similarly, diclofenac treatment decreased LAMP2A protein levels in HepG2 cells and MPH. But, the levels of hsc70 did not change in any of the groups. The protein level of LAMP2A diminished over time. However, the mRNA level of LAMP2A was not altered by diclofenac, which suggests the possibility that diclofenac abrogates the stability of LAMP2A. (Figure 15)

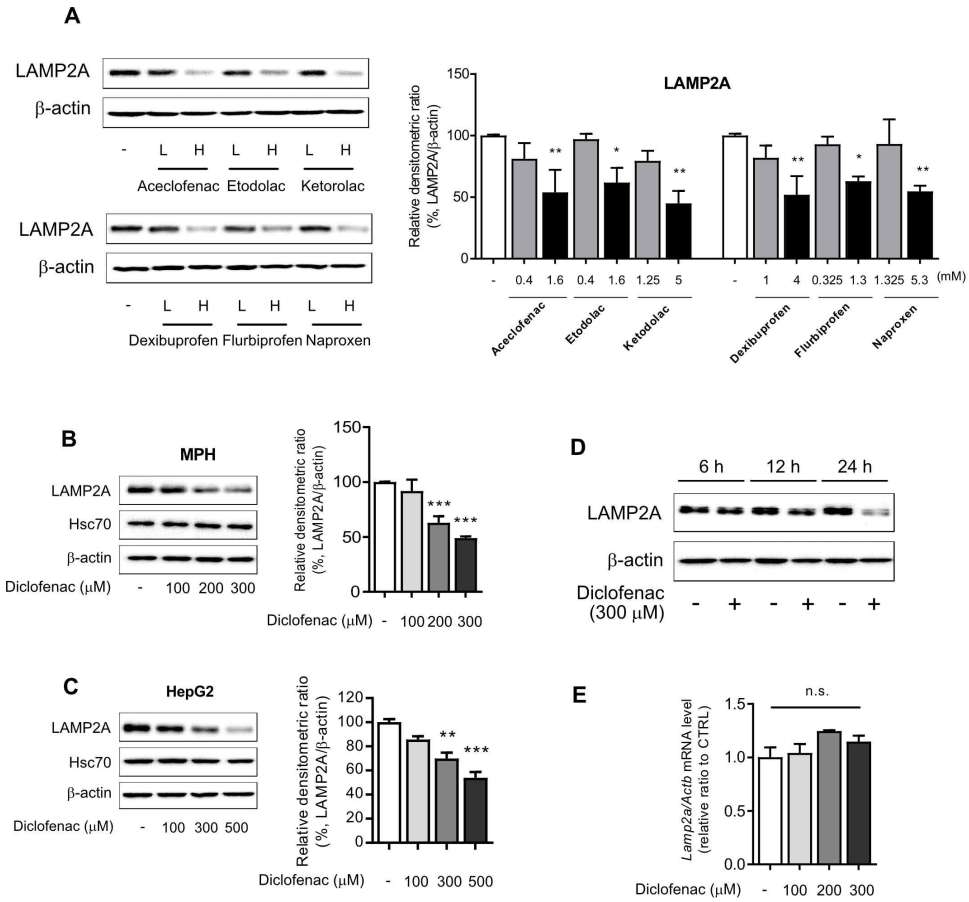

Figure 15. Several NSAIDs including diclofenac decreased the protein level of LAMP2A.

(A) HepG2 cells were treated with the indicated concentration of NSAIDs for 24 h, and the levels of LAMP2A were analyzed by western blotting (L; Low concentration, H; High concentration). (B, C) Western blot analysis of LAMP2A and Hsc70 in MPH and HepG2 cells treated with the indicated concentration of diclofenac for 24 h. The right panels show the quantification of the LAMP2A level. (D) Western blot analysis of LAMP2A in HepG2 cells treated with

diclofenac (300 μM) at the indicated time point. (E) mRNA was extracted from MPH treated with the indicated concentration of diclofenac for 24 h, and mRNA levels of *Lamp2a* were analyzed by qRT-PCR. Data are presented as mean ± SD of at least 3 independent experiments, as analyzed by one-way ANOVA followed by Tuckey's test. **p < 0.01, and ***p < 0.001, compared to the control group. n.s.; non-significant relative to the control group.

3.3.2. COX inhibitory activity was not responsible for the CMA impairment by NSAID

The anti-inflammatory activity of NSAIDs derived from COX inhibition is well established. Most of the NSAID's effects are caused by their ability to inhibit the enzyme COX early in the synthetic pathway.

To rule out whether CMA impairment by NSAIDs is associated with inhibition of cyclooxygenase (COX), ibuprofen isomers were used to determine the correlation between COX inhibition and CMA activity. The effects of (S)- and (R)-ibuprofen were compared, which is active and inactive on the COX enzyme, respectively. Both stereoisomers and a racemic mixture of ibuprofen accumulated intracellular lipid and inhibited CMA to a similar degree. Moreover, no significant change of CMA marker proteins was observed when the COX1 gene was knockdown in MPH. These results suggest that COX inhibitory activity is not responsible for the CMA impairment by NSAID. (Figure 16)

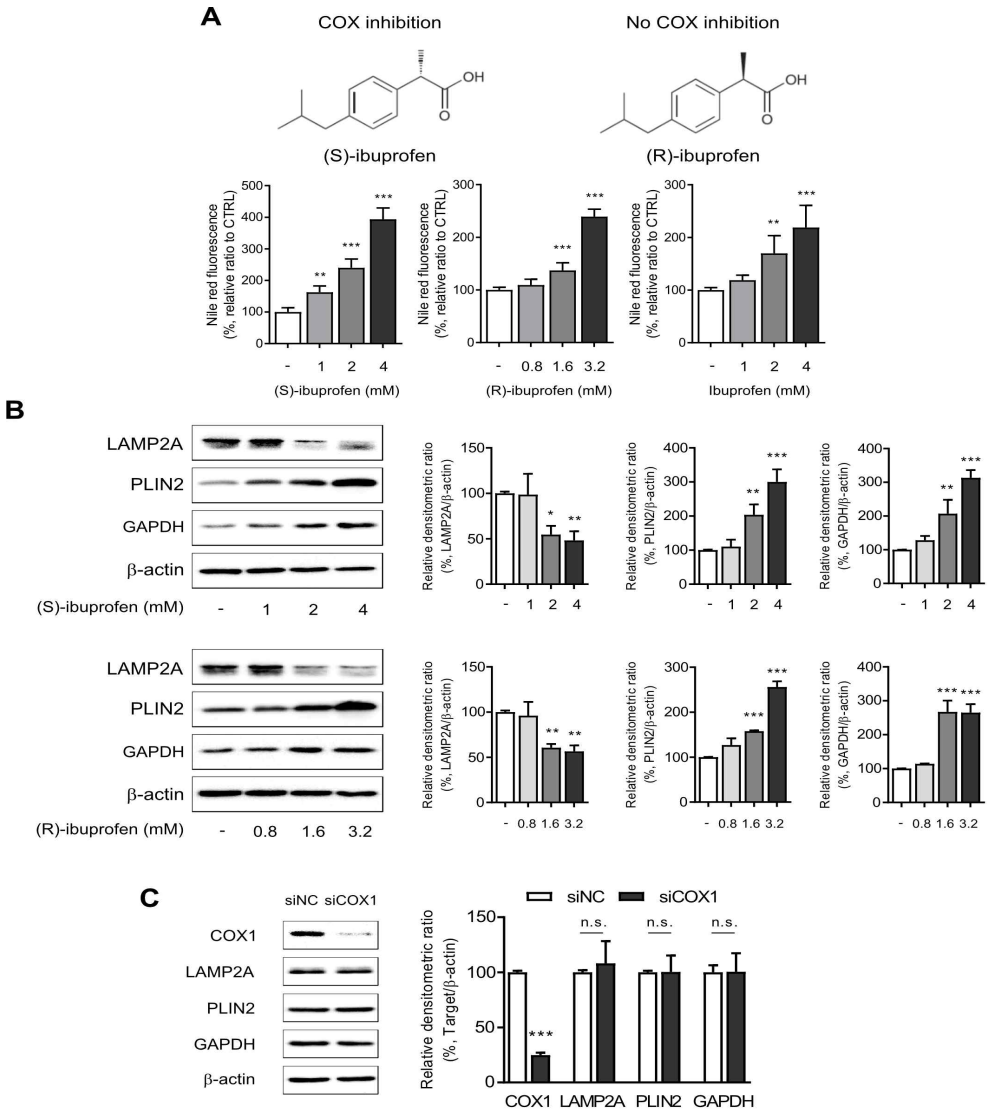

Figure 16. CMA impairment by NSAIDs was independent of COX inhibition

(A) Chemical structure of (S)- and (R)- ibuprofen. HepG2 cells were incubated with (S)-ibuprofen or (R)-ibuprofen or racemic mixture of ibuprofen at the indicated concentration for 24 h. Intracellular lipid

concentrations were quantified using Nile-red dye; excitation and emission wavelengths of 486 and 528 nm, respectively. (B) The protein levels of LAMP2A, PLIN2, and GAPDH were measured by western blot analysis. The right panels show the densitometric quantification of target proteins. (C) MPH were transfected with control or COX1 siRNA. The protein levels of COX1, COX2, LAMP2A, PLIN2, and GAPDH were measured by western blot analysis. Data are presented as mean ± SD of at least 3 independent experiments, as analyzed by one-way ANOVA followed by Tuckey's test. **$p < 0.01$, and ***$p < 0.001$, relative to the control group.

3.3.3. The inhibition of CMA by diclofenac suppressed the degradation of CMA substrates in the lysosome

In Figure 15, the level of LAMP2A decreased by treatment of diclofenac. LAMP2A works as a receptor for protein substrates at the lysosomal membrane. To address whether diclofenac diminished LAMP2A in the lysosome, LAMP2A levels in the lysosomal fraction were analyzed. Diclofenac treatment markedly decreases LAMP2A protein levels in lysosomal fractions (Figure 17).

Based on these findings, whether the inhibition of CMA by diclofenac suppressed the degradation of CMA substrates was evaluated. A comparative analysis was performed by measuring the lysosomal levels of the CMA substrates in cells in the absence or presence of leupeptin. Leupeptin is used as an inhibitor of lysosomal proteolysis. If the protein degraded in lysosomes in a LAMP2A-dependent manner, their lysosomal levels increased upon proteolysis inhibition in the leupeptin-only group. As expected, the CMA substrates, GAPDH, PLIN2, and pyruvate kinase were accumulated in the lysosome of leupeptin-treated cells and did not increase in the lysosome by the cotreatment with diclofenac and leupeptin. These data indicate that blockade of LAMP2A-mediated lysosomal uptake by diclofenac hinders the degradation of PLIN2 (Figure 17).

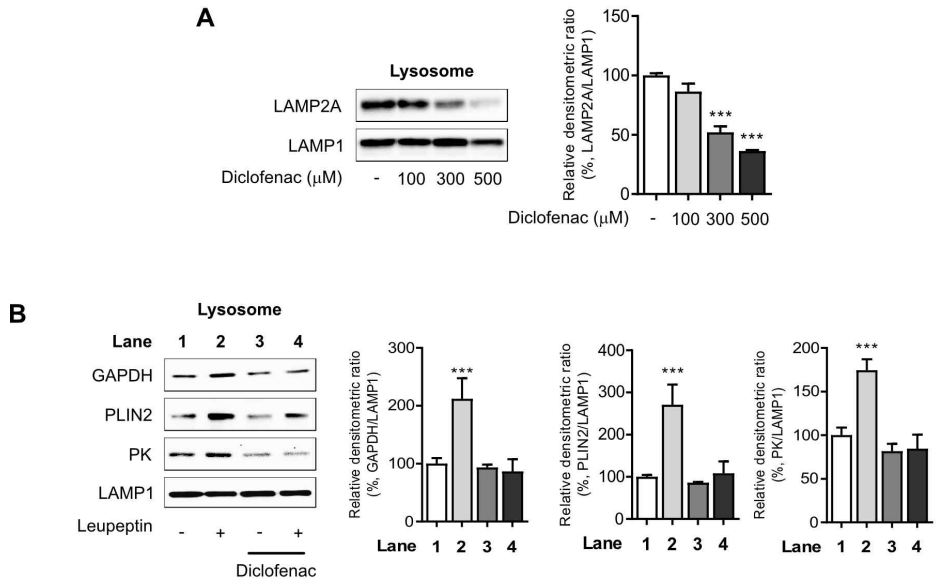

Figure 17. The inhibition of CMA by diclofenac suppressed the degradation of CMA substrates in the lysosome

(A) LAMP2A and LAMP1 were measured in lysosomal fractions isolated from diclofenac-treated HepG2 cells. The right panel shows the quantification of the LAMP2A level. (B) HepG2 cells were treated with diclofenac (300 μM) and leupeptin (100 μM) and the indicated CMA substrates (GAPDH, PLIN2, PK; Pyruvate kinase) were determined in the lysosomal fraction using western blotting. Representative western blot images and the densitometric quantification of proteins are shown. Data are presented as mean ± SD of at least 3 independent experiments, as analyzed by one-way ANOVA followed by Tuckey's test. ***$p < 0.001$, relative to the control group.

3.3.4. The inhibition of CMA by diclofenac resulted in decreased translocation of CMA substrates.

To further investigate whether the CMA inhibition by diclofenac resulted in the impairment of CMA substrates to the lysosome, the fusion between PLIN2 and lysosomes was analyzed by examining the colocalization of PLIN2 and LAMP1 (a marker of lysosome and late endosomes) in the absence and presence of diclofenac and/or oleate in MPH. The cells treated with oleate shows increased colocalization of PLIN2 with LAMP1. On the other hand, the colocalization of PLIN2 and lysosomes in the cells treated with diclofenac was markedly decreased under both normal and lipogenic conditions. In conclusion, diclofenac-induced CMA inhibition impairs the translocation of CMA substrates to the lysosome (Figure 18).

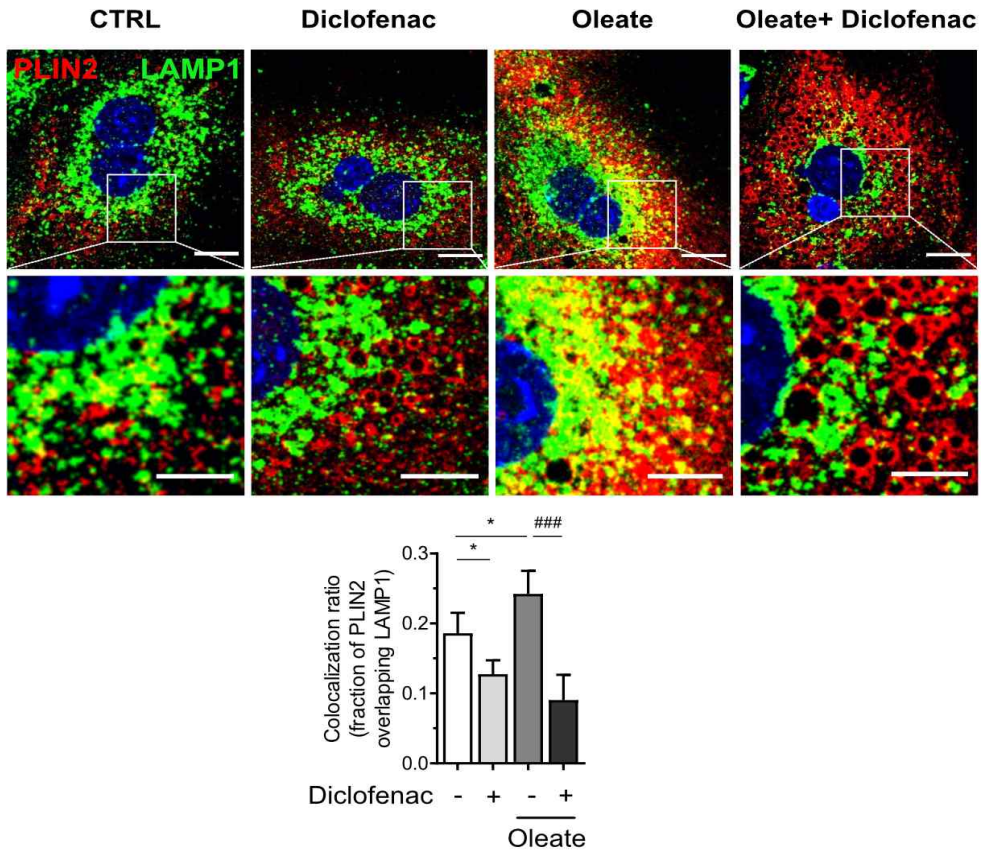

Figure 18. The inhibition of CMA by diclofenac resulted in decreased CMA substrates translocation.

MPH were treated with diclofenac (300 μM) and oleate (100 μM) for 24 h, and PLIN2 and LAMP1 expression were determined by immunofluorescence staining. PLIN2 (red), LAMP1 (green), DAPI (blue). (Scale bars; 20 μm) Representative fluorescent images of the cells and the zoomed images magnified from the small boxed areas in each image are shown (Scale bars; 10 μm). Percentages of co-localization of PLIN2 with LAMP1 are shown in bottom panel. Data are presented as mean ± SD of at least 3 independent experiments, as analyzed by one-way ANOVA followed by Tuckey's test. *$p < 0.05$, **$p < 0.01$, and ***$p < 0.001$, relative to the control group. ###$p < 0.001$, relative to the indicated group. n.s.; non-significant relative to the control group.

3.4. CMA reactivation reduces diclofenac-induced lipid accumulation in hepatocytes

3.4.1. The development of CMA reactivation *in vitro* models for the study of diclofenac-induced CMA inhibition.

CMA reactivation *in vitro* model system was developed by using a chemical CMA activator and LAMP2A overexpression vector. It is reported that retinoic acid receptor α (RARα) inhibits CMA and RAR α antagonist, AR7 specifically activates CMA without affecting macroautophagy (Anguiano *et al.* 2013). Both chemical CMA activator and LAMP2A overexpression vector increased the expression of LAMP2A (Figure 19).

To determine CMA activity, the photoactivatable fluorescence-based cell assay was used to track lysosomal uptake (Koga *et al.* 2011). A cell-based assay was developed to monitor the rate of cellular clearance of CMA substrates which consists of a CMA recognition motif (KFERQ). The initial fluorescence intensity after photoactivation reflects the basal level of substrate proteins. As CMA pathway was activated, CMA substrates were translocated to the lysosome and changed the mostly diffuse red fluorescence pattern to a punctuate pattern. The number of fluorescent-puncta significantly decreased after exposure to diclofenac compared with the vector control cells.

To confirm the CMA inhibitory effect of diclofenac, LAMP2A was stained using an antibody to LAMP2A in MPH. Fluorescence

microscopy demonstrated that treatment of diclofenac decreased the fluorescence of LAMP2A. Taken together, these results suggest that CMA reactivation restores the inhibition of CMA via diclofenac (Figure 20).

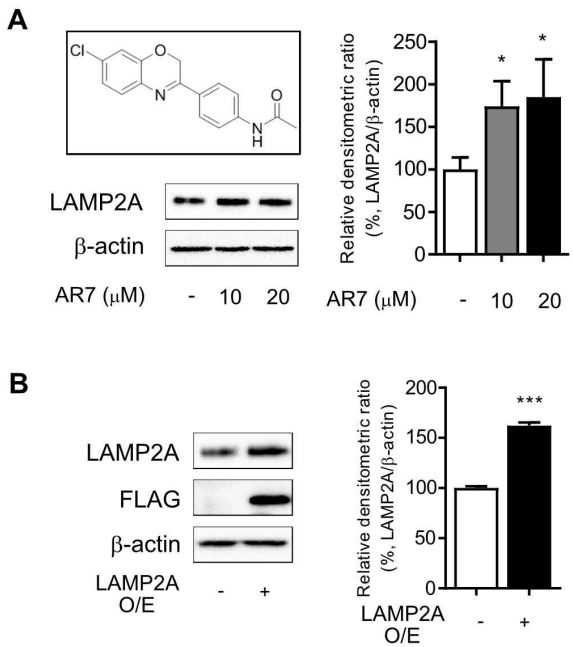

Figure 19. The development of CMA reactivation *in vitro* models

(A) Molecular structure of AR7 (chemical CMA activator). The protein level of LAMP2A were measured in MPH by western blot analysis. The densitometric quantification of the LAMP2A level is shown. (B) MPH were transfected with pCMV-LAMP2A plasmid. Western blot analysis with antibodies against LAMP2A and FLAG. the densitometric quantification of the LAMP2A level is shown. Data are presented as mean ± SD of at least 3 independent experiments, as analyzed by student's t-test. *p < 0.05, and ***p < 0.001, relative to the control group.

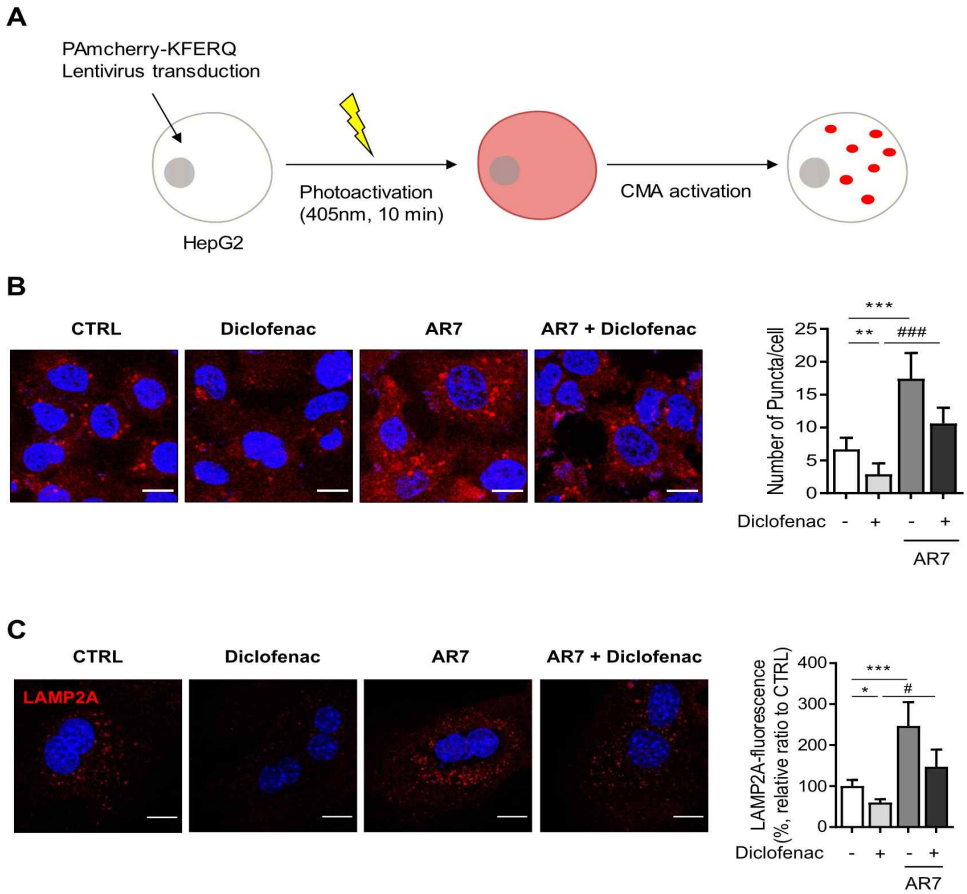

Figure 20. CMA reactivation reduced diclofenac-induced inhibition of CMA

(A) Scheme of the experimental design to monitor CMA activity in cultured cells using the PAmcherry-KFERQ reporter. (B) HepG2 cells were treated with diclofenac (300 μM) and AR7 (10 μM) for 24 h followed by transfection with pSIN-PAmCherry-KFERQ-NE plasmid. Representative fluorescent images and quantification of PAmCherry-KFERQ puncta are shown (Red puncta; PAmCherry, Blue; DAPI). (C) MPH were incubated with diclofenac (300 μM) or AR7 (10 μM) for 24 h. Confocal microscopy images was analyzed to

detect LAMP2A. Representative fluorescent images and quantitative data of the cells are shown (Scale bars: 20 μm). Data are presented as mean ± SD of at least 3 independent experiments, as analyzed by one-way ANOVA followed by Tuckey's test. *p < 0.05, **p < 0.01, and ***p < 0.001, relative to the control group. #p < 0.05, ###p < 0.001, relative to the indicated group.

3.4.2. CMA reactivation reversed the diclofenac-induced failure in the degradation of CMA substrates

In Figure 20, it was shown that CMA reactivation by AR7 reversed the effect of diclofenac on CMA inhibition. To investigate whether reactivation of CMA reverses diclofenac-induced accumulation of CMA substrates, diclofenac and/or AR7 were treated in MPH. AR7 reversed the diclofenac-induced failure in the degradation of CMA substrates such as PLIN2 and GAPDH. Also, the level of LAMP2A was reduced by diclofenac and reversed by the treatment of AR7.

Then, the up-regulation of CMA activity by amplification of LAMP2A was also measured. The overexpression of LAMP2A by genetic vector transfection reversed the accumulation of CMA by diclofenac treatment (Figure 21).

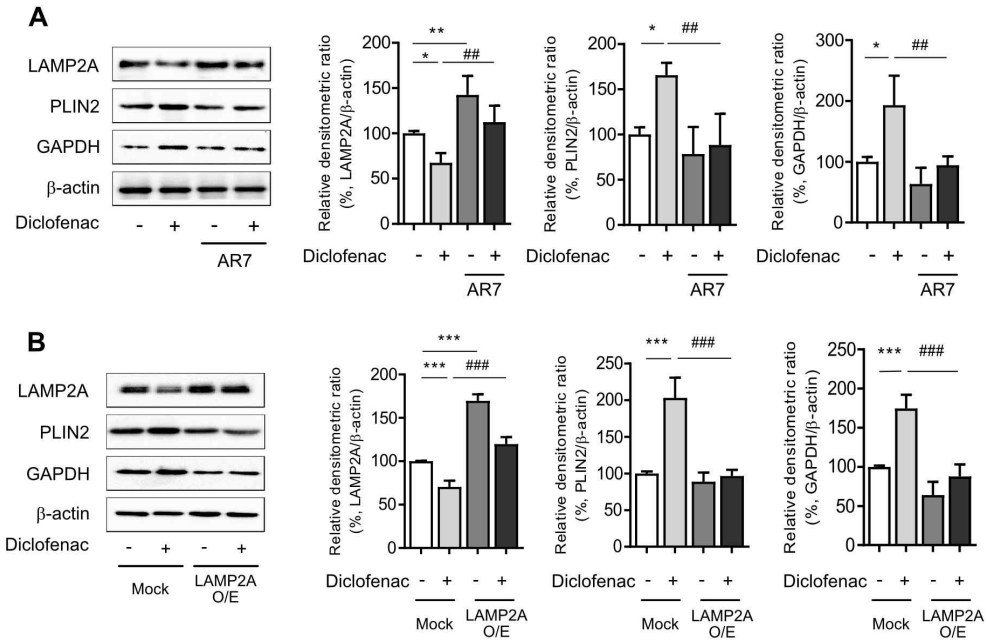

Figure 21. CMA reactivation reversed the diclofenac-induced failure in the degradation of CMA substrates

(A) The protein levels of LAMP2A, PLIN2, and GAPDH were measured in MPH by western blot analysis. Representative western blot images and the densitometric quantification of proteins are shown. (B) MPH were transfected with pCMV-LAMP2A plasmid and were incubated with diclofenac for 24 h. Western blot analysis with antibodies against LAMP2A, PLIN2 and GAPDH and the densitometric quantification of the PLIN2 and GAPDH level are shown. Data are presented as mean ± SD of at least 3 independent experiments, as analyzed by one-way ANOVA followed by Tuckey's test. *$p < 0.05$, **$p < 0.01$, and ***$p < 0.001$, relative to the control group. ##$p < 0.01$, ###$p < 0.001$, relative to the indicated group.

3.4.3. CMA reactivation decreased the lipid accumulation induced by diclofenac

To identify whether reactivation of CMA reverses diclofenac-induced lipid accumulation in hepatocytes, MPH were treated with diclofenac and/or AR7, and changes in lipid droplets were detected by imaging analysis using BODIPY 493/503 dye. AR7 treatment reversed the diclofenac-induced intracellular lipid accumulations. Also, biochemical triglyceride analysis revealed that AR7 treatment markedly decreased the lipid accumulation induced by diclofenac. Similar results were obtained in cells transfected with a LAMP2A-expressing plasmid. Overexpression of LAMP2A restored the lipid accumulation induced by diclofenac treatment. Together, these results reveal that the incurring of the defect in LAMP2A-mediated CMA activity is a significant factor underlying the lipid accumulation by diclofenac (Figure 22).

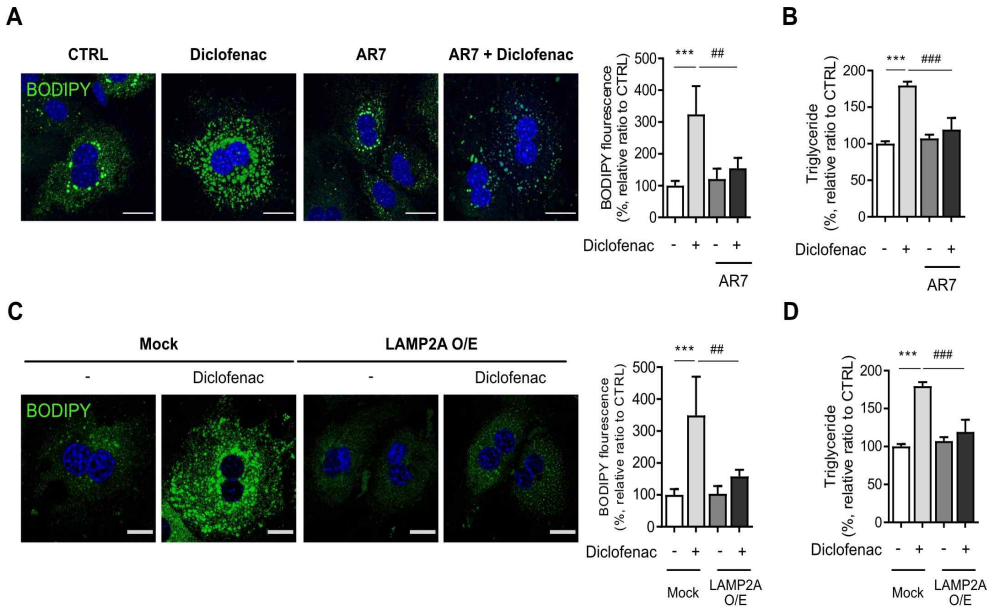

Figure 22. CMA reactivation decreased the lipid accumulation induced by diclofenac

(A) MPH were incubated with diclofenac (300 μM) and AR7 (10 μM) for 24 h. Intracellular lipid droplets (LDs) were determined by BODIPY 493/503 fluorescence (green). Nuclei were stained with DAPI (blue) (Scale bars: 20 μm). (B) TG concentration in MPH was quantified using an enzymatic kit. (C) MPH were transfected with pCMV-LAMP2A plasmid and were incubated with diclofenac for 24 h. Intracellular LDs were determined by BODIPY 493/503 fluorescence (green). Nuclei were stained with DAPI (blue) (Scale bars: 20 μm). (D) TG concentration in MPH was quantified using the enzymatic kit. Data are presented as mean ± SD of at least 3 independent experiments, as analyzed by one-way ANOVA followed by Tuckey's test. ***p < 0.001, relative to the control group. ##p < 0.01, ###p < 0.001, relative to the indicated group.

3.4.4. CMA inhibition by diclofenac was independent of macroautophagy inhibition or oxidative stress

In the previous report, LDs are also susceptible to degradation by macroautophagy. Since it was reported that NSAIDs inhibit macroautophagy (Jung *et al.* 2020), whether inhibition of macroautophagy also contributes to diclofenac-induced lipid accumulation was investigated. To examine whether restoring macroautophagy activity affects diclofenac-induced lipid accumulation, clioquinol and rapamycin were used, both of which have been proven to activate autophagic flux in diclofenac-treated cells. Unlike AR7, however, treatment of clioquinol did not reverse the expression level of the LAMP2A or CMA substrates, and neither did it reverse lipid accumulation by diclofenac. Rapamycin, a macroautophagy activator, also did not alleviate the inhibition of CMA and lipid accumulation by diclofenac. These data indicate that diclofenac-induced lipid accumulation is independent of non-CMA autophagy (Figure 23).

Previous studies suggest that diclofenac increases mitochondrial ROS, which is responsible for the suppression of autophagic flux. Another previous study demonstrated that diclofenac impairs autophagic flux via oxidative stress. To investigate whether ROS generated by diclofenac affects CMA, the parameters of CMA were measured following co-treatment with ROS scavengers. Although N-acetylcysteine or Mito-tempo reversed the autophagy suppressed by diclofenac, the levels of the proteins associated with CMA were not altered in MPH (Figure 24).

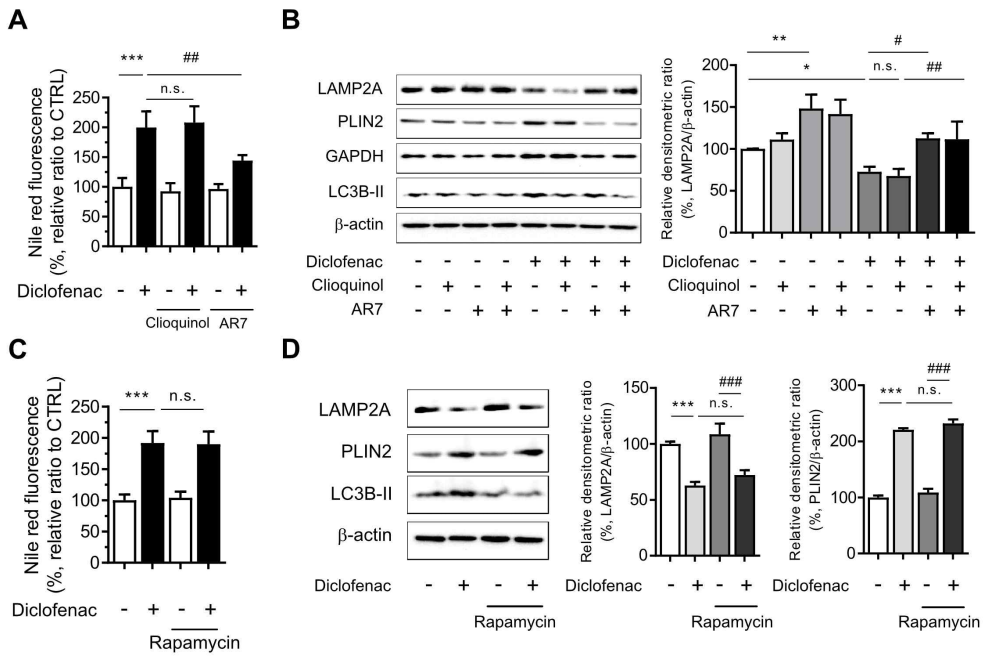

Figure 23. CMA inhibition by diclofenac was independent of macroautophagy inhibition

(A, B) MPH were incubated with diclofenac (300 μM) or Clioquinol (10 μM), AR7 (10 μM) for 24 h. (A) Intracellular lipid concentrations were quantified using Nile-red dye; excitation and emission wavelengths of 486 and 528 nm, respectively. (B) The protein levels of LAMP2A, PLIN2, GAPDH, and LC3B-Ⅱ were measured by western blot analysis. Representative Western blot images and the relative quantification of LAMP2A are shown. (C, D) MPH were incubated with diclofenac (300 μM) or Rapamycin (0.5 μM) for 24 h. (C) Intracellular lipid concentrations were quantified using Nile-red dye; excitation and emission wavelengths of 486 and 528 nm, respectively. (D) The protein levels of LAMP2A, PLIN2, and LC3B-Ⅱ were measured by western blot analysis. Representative western blot

images and the densitometric quantification of proteins are shown. Data are presented as mean ± SD of at least 3 independent experiments, as analyzed by one-way ANOVA followed by Tuckey's test. *p < 0.05, **p < 0.01, ***p < 0.001, relative to the control group. #p < 0.05, ##p < 0.01, ###p < 0.001, relative to the indicated group. n.s.; non-significant relative to the indicated group.

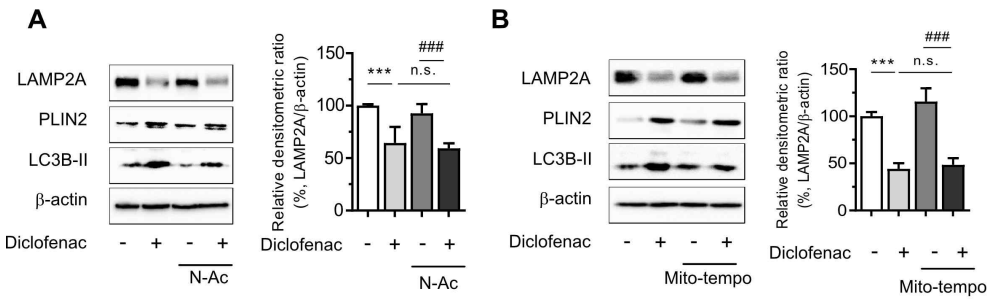

Figure 24. CMA inhibition by diclofenac was independent of oxidative stress

(A, B) MPH were pretreated with N‐acetylcysteine (N-Ac;5 mM) or Mito-Tempo (10 μM) for 1 hr, and further incubated with diclofenac (300 μM; 24 hr). The protein levels of LAMP2A, PLIN2, and LC3B-Ⅱ were measured by western blot analysis. Representative Western blot images and the relative quantification of LAMP2A are shown. Data are presented as mean ± SD of at least 3 independent experiments, as analyzed by one-way ANOVA followed by Tuckey's test. ***p < 0.001, relative to the control group. ###p < 0.001, relative to the indicated group. n.s.; non-significant relative to the indicated group.

3.5. Diclofenac decreased the level of LAMP2A via SNX10-mediated activation of CTSA maturation

3.5.1. Diclofenac induced the expression of SNX10 and the mature form of CTSA

Next, the mechanism by which diclofenac decreases LAMP2A protein levels was investigated. Based on the results that the transcription levels of LAMP2A were not changed by diclofenac treatment (Figure 15), it was hypothesized that the protein stability of LAMP2A might be affected.

Active CTSA interacts with LAMP2A on the lysosomal membrane and stimulates its degradation. According to You *et al.*, deficiency of SNX10 increases the stability of LAMP2A by inhibiting the trafficking and maturation of CTSA in the lysosome (You *et al.* 2018). To examine whether the inhibition of CMA by diclofenac was due to the increased expression of SNX10 and the mature form of CTSA, the level of SNX10 and the mature form of CTSA were measured. Diclofenac treatment induced the expression of SNX10 at the transcriptional level and increased the mature form of CTSA.

To verify that the impairment of CMA substrates degradation by diclofenac was attributed to increased expression of SNX10, activation of CTSA, siRNA knockdown experiment was performed. When the expression of CTSA and SNX10 was blocked with siRNA, diclofenac did not affect CMA substrates accumulation. These results imply that diclofenac decreased CMA activity via SNX10-mediated CTSA maturation (Figure 25).

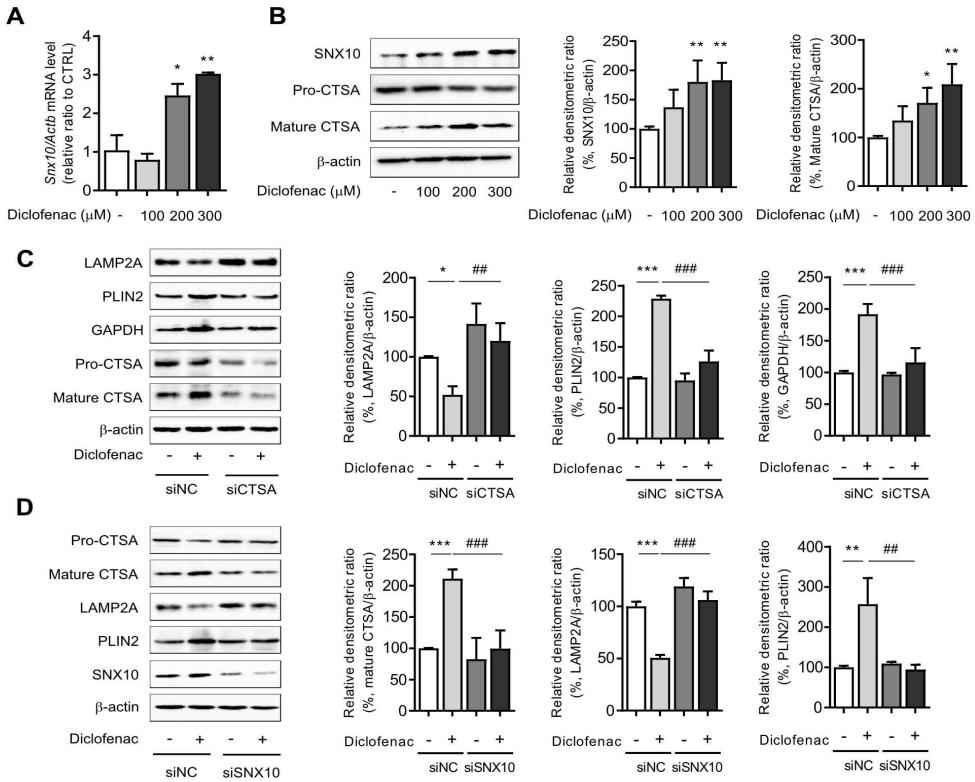

Figure 25. Diclofenac induced the expression of SNX10 and the mature form of CTSA

(A) MPH were incubated with diclofenac (300 μM) for 24 h, and mRNA was isolated and subjected to qRT-PCR analysis to measure sorting nexin 10 (SNX10) mRNA expression. (B) The level of SNX10, pro-CTSA, and mature CTSA was measured by western blot analysis in MPH treated with diclofenac. Representative western blot images and the densitometric quantification of proteins are shown. (C) MPH were transfected with control or CTSA siRNA. The protein levels of LAMP2A, PLIN2, GAPDH, pro-CTSA and mature CTSA were measured by western blot analysis. (D) MPH were transfected with control or SNX10 siRNA. The protein levels of LAMP2A,

PLIN2, pro-CTSA, mature CTSA and SNX10 were measured by western blot analysis. Data are presented as mean ± SD of at least 3 independent experiments, as analyzed by one-way ANOVA followed by Tuckey's test. *p < 0.05, **p < 0.01, and ***p < 0.001, relative to the control group. ##p < 0.01, ###p < 0.001, relative to the diclofenac-treated group.

3.5.2. Knockdown of CTSA and SNX10 decreased the lipid accumulation induced by diclofenac

To investigate the role of SNX10 and CTSA in diclofenac-induced lipid accumulation, MPH were treated with diclofenac and/or CTSA, SNX10 knockdown siRNA. Changes in lipid droplets were detected by imaging analysis using BODIPY 493/503 dye. When CTSA siRNA or SNX10 siRNA were transfected, intracellular lipid accumulation by diclofenac was recovered. Also, biochemical triglyceride analysis revealed that knockdown of CTSA and SNX10 significantly decreased the lipid accumulation induced by diclofenac. These results indicate that subsequent intracellular lipid accumulation by diclofenac is attributed to increased expression of SNX10, activation of CTSA (Figure 26).

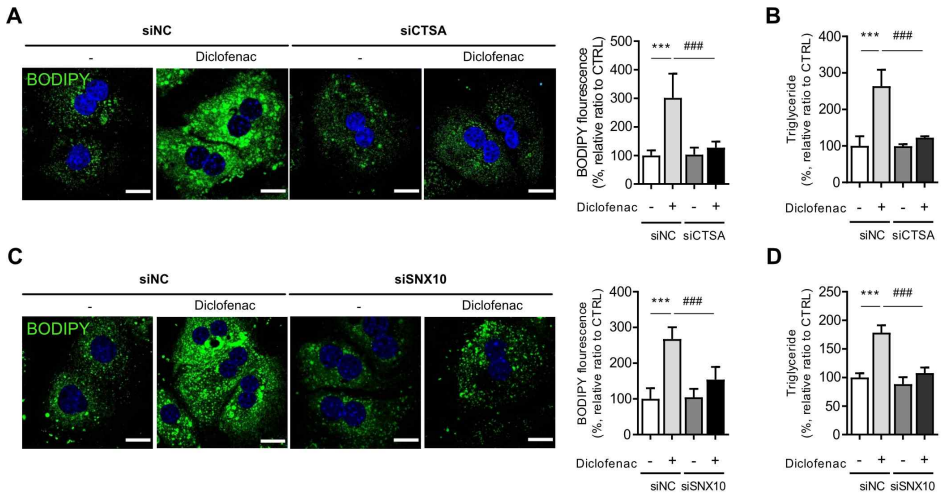

Figure 26. Knockdown of CTSA and SNX10 decreased the lipid accumulation induced by diclofenac

(A, B) MPH were transfected with control or CTSA siRNA and were incubated with diclofenac (300 μM) for 24 h. (A) Intracellular LDs were determined by BODIPY 493/503 fluorescence (green). Nuclei were stained with DAPI (blue) (Scale bars: 20 μm). (B) TG concentration was quantified using an enzymatic kit. (C, D) MPH were transfected with control or SNX10 siRNA and were incubated with diclofenac for 24 h. (C) Intracellular LDs were determined by BODIPY 493/503 fluorescence (green). Nuclei were stained with DAPI (blue) (Scale bars: 20 μm). (D) TG concentration was quantified using the enzymatic kit. Data are presented as mean ± SD of at least 3 independent experiments, as analyzed by one-way ANOVA followed by Tuckey's test. ***$p < 0.001$, relative to the control group. ###$p < 0.001$, relative to the diclofenac-treated group.

3.6. Endoplasmic reticulum (ER) stress was responsible for increase of SNX10 by NSAIDs

3.6.1 SNX10 was increased in liver disease model and tunicamycin-induced ER stress model

The mechanism by which diclofenac increases the expression of SNX10 was explored. A recent study by You *et al.* demonstrated the role of SNX10 in alcohol-induced liver steatosis. Thus, a microassay analysis was performed using Gene Expression Omnibus (GEO) database in various liver disease models. Microarray data has shown that the level of SNX10 is significantly elevated in the mice fed a methionine- and choline-deficient plus high-fat (MCD+HF) diet. The NCBI GEO database has revealed that SNX10 is highly expressed in the human liver of NAFLD patients (accession numbers GSE25907, GSE48452). Interestingly, SNX10 is significantly increased in the tunicamycin-induced ER stress mouse model (accession numbers GSE167299). These data demonstrate that increased expression of SNX10 involves a link with liver disease and ER stress (Figure 27).

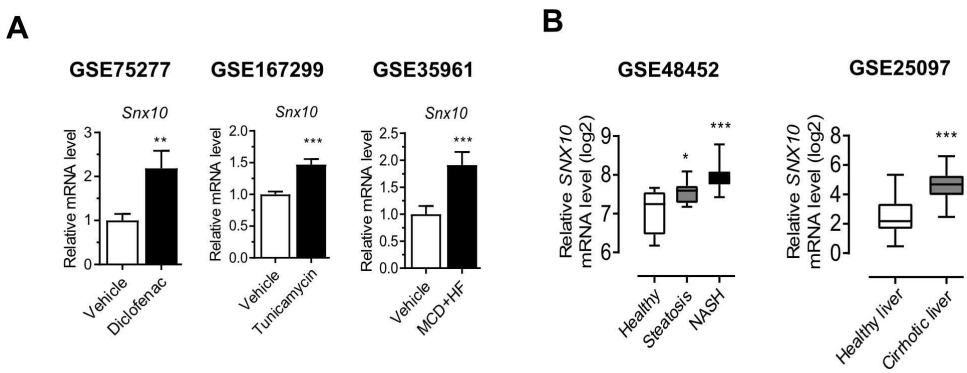

Figure 27. SNX10 was increased in liver disease model and tunicamycin-induced ER stress model

(A) Microarray data from diclofenac-treated mouse model or tunicamycin-treated mouse model or methionine-choline deficient (MCD) diet with high-fat (HF) mouse modeol were analyzed by the GEO integrated analysis tool GEO2R. (B) Microarray data from human simple steatosis, non-alcoholic steatohepatits or human liver cirrhosis were analyzed by the GEO integrated analysis tool GEO2R Data are presented as means ± SD. * $p < 0.05$, **$p < 0.01$, and ***$p < 0.001$, represent significant differences relative to the vehicle or health liver group using Student's t-test.

3.6.2. ER stress induced the expression of SNX10 and the inhibition of CMA in hepatocytes.

In the previous data (Figure 27), ER stress induced the expression of SNX10 in tunicamycin-treated mice. And, the transcription factor binding sites of SNX10 were analyzed using QIAGEN (GeneCards.org) and the ChIPseq database on GTRD. C/EBP α/β and C/EBP-homologous protein (CHOP) were identified as possible SNX10 transcription factors (data not shown). Therefore, it was hypothesized that endoplasmic reticulum stress responses might be associated with SNX10 expression. Diclofenac treatment upregulated the protein levels of the ER stress markers, the glucose-regulated protein-78 (GRP78/BiP), and CHOP together with those of SNX10 in a time-dependent manner. When the ER stress responses were induced in the cells with tunicamycin, the expression of SNX10 was increased significantly concomitant with the lowered expression of LAMP2A. Thereafter, qRT-PCR was performed under various stresses in MPH, including hormonal (forskolin; FSK), inflammatory (transforming growth factor-β; TGFβ), nutritional (high glucose; Glc), diclofenac and tunicamycin. Interestingly, *Snx10* and *Chop* mRNA levels were elevated explicitly under diclofenac and tunicamycin treatment indicating a tight correlation between SNX10 and hepatic ER stress levels.

Collectively, these results suggest that diclofenac and tunicamycin-induced ER stress increased the expression of SNX10, leading to impairment of CMA in hepatocytes (Figure 28)

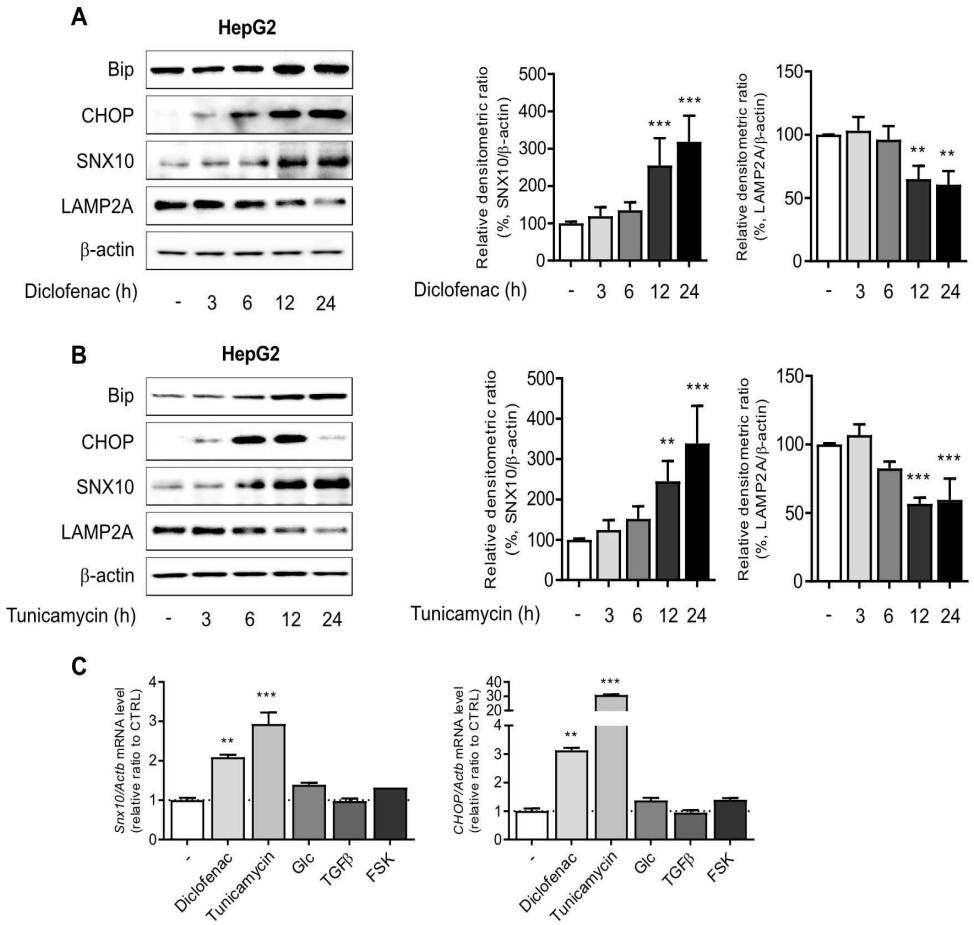

Figure 28. ER stress induced the expression of SNX10 and the inhibition of CMA in hepatocytes.

(A, B) HepG2 cells were treated with diclofenac (300 μM) or tunicamycin (3 μg/ml) at the indicated time point and subjected to western blot analysis with antibodies against Bip, CHOP, and SNX10 and LAMP2A and the densitometric quantification of the SNX10 and LAMP2A level are shown. (C) Relative mRNA levels of *Snx10* and *CHOP* in MPH treated with diclofenac (300 μM) or tunicamycin (3 μg/ml), glucose (Glu, 5 mM), transforming growth factor β (TGFβ, 10

ng/ml), forskolin (FSK, 1 μM). Data are presented as mean ± SD of at least 3 independent experiments, as analyzed by one-way ANOVA followed by Tuckey's test. **p < 0.01, and ***p < 0.001, relative to the control group.

3.6.3. The release of intracellular Ca^{2+} is important for diclofenac-induced upregulation of SNX10

The storage and release of Ca^{2+} are critical physiological functions of the ER. Disrupted ER homeostasis activates the unfolded protein response (UPR). In previous reports, ER stress response is involved in NSAID-induced cell death and toxicity where Ca^{2+}-dependent CHOP induction plays an important role.

To assess whether NSAIDs elevate intracellular Ca^{2+} levels in liver cells, NSAIDs were treated on HepG2 cells loaded with fluo-3 AM, the calcium-binding fluorescent dye. The intracellular Ca^{2+} concentration was significantly increased by treatment of diclofenac in a dose-dependent manner. All of the CMA-inhibiting NSAIDs showed similar results.

To determine whether increased intracellular Ca^{2+} is essential for diclofenac-induced upregulation of SNX10, BAPTA-AM, a cell-permeable intracellular Ca^{2+} chelator, was used. BAPTA-AM alleviated diclofenac-induced ER stress response, SNX10 expression, and CMA inhibition. These data indicate that diclofenac induced the release of intracellular Ca^{2+}, leading to upregulation of SNX10 (Figure 29).

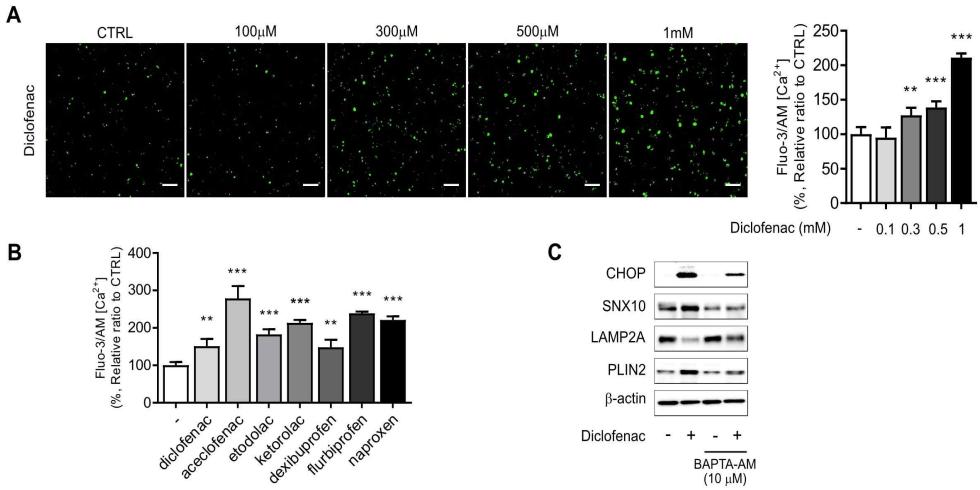

Figure 29. The release of intracellular Ca^{2+} was important for diclofenac-induced upregulation of SNX10

(A) HepG2 cells were incubated with the indicated concentration of diclofenac for 30 min, and intracellular Ca^{2+} level was analyzed by fluo-3 AM. The fluorescence intensity was calculated using an Cytation3 cell imaging microplate reader (Scale bars: 100 μm). (B) HepG2 cells were treated with NSAIDs (Diclofenac; 0.5 mM, Aceclofenac; 1.6 mM, Etodolac; 1.6 mM, Ketodolac; 5 mM, Dexibuprofen; 4 mM, Flurbiprofen; 1.3 mM, Naproxen; 5.3 mM) and intracellular Ca^{2+} level was analyzed by fluo-3 AM. The fluorescence intensity was calculated using an Incucyte cell imaging microplate reader. (C) HepG2 cells were pretreated with BAPTA-AM (10 μM) for 1 h before diclofenac treatment (300 μM). The protein levels of CHOP, SNX10, LAMP2A and PLIN2 were measured by western blot analysis. Data are presented as mean ± SD of at least 3 independent experiments, as analyzed by one-way ANOVA followed by Tuckey's test. **$p < 0.01$, and ***$p < 0.001$, relative to the control group.

3.6.4. ER stress inhibitors reversed diclofenac-induced ER stress on SNX10 and LAMP2A expression

ER stress can be attenuated with small-molecule chemical chaperones like chemical chaperone 4-phenylbutyric acid (4-PBA) and tauroursodeoxycholic acid (TUDCA). Chemical chaperones mimic native chaperones, promoting folding, preventing aggregation, and restoring trafficking of misfolded proteins (Dromparis *et al.* 2013).

To determine the effect of diclofenac-induced ER stress on SNX10 and LAMP2A expression, ER stress inhibitors were used. Co-incubation with ER stress inhibitors 4-PBA or TUDCA during diclofenac exposure reversed the change of diclofenac-induced SNX10 upregulation and LAMP2A downregulation. Thus, the results demonstrated that ER stress is associated with the induction of SNX10 and the inhibition of CMA activity. (Figure 30)

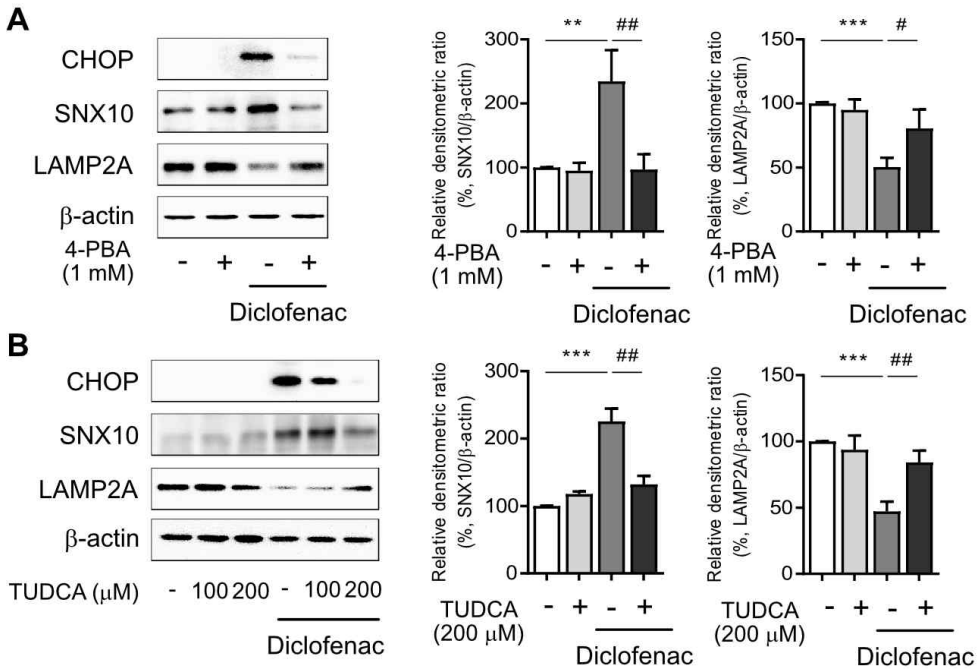

Figure 30. ER stress inhibitors reversed diclofenac-induced ER stress on SNX10 and LAMP2A expression

(A, B) HepG2 cells were treated with diclofenac (300 μM) in the presence or absence of 4-phenylbutyrate (4-PBA, 1 mM; 1 hr pretreatment) or taurodeoxycholic acid (TUDCA, 100, 200 μM; 2 hr pretreatment) and subjected to western blot analysis with antibodies against CHOP, SNX10, and LAMP2A. The densitometric quantification of SNX10 and LAMP2A are shown in the right panels. Data are presented as mean ± SD of at least 3 independent experiments, as analyzed by one-way ANOVA followed by Tuckey's test. **$p < 0.01$, and ***$p < 0.001$, relative to the control group. #$p < 0.05$, ##$p < 0.01$, relative to the diclofenac-treated group.

3.6.5. CHOP-dependent SNX10 induction was responsible for the lipid accumulation by diclofenac.

In contrast to previous findings, Li *et al.* reported that ER stress induces the CMA pathway in SN4741 cells (a nigral dopaminergic cell line) by recruiting mitogen-activated protein kinase 4 (MKK4) to phosphorylate LAMP2A for CMA activation (Li *et al.* 2017). Therefore, the levels of SNX10 and LAMP2A were evaluated in MPH and SN4741 cells after treatment of diclofenac or tunicamycin.

The expression of SNX10 was deficient in SN4741 cells. Diclofenac or tunicamycin downregulated the level of LAMP2A in MPH. However, the LAMP2A level was upregulated in SN4741 cells (Figure 31).

To further identify the pathway that mediates the ER stress-induced CMA inhibition in HepG2 cells, the main mediators of UPR were inhibited by using siRNA of CHOP, ATF6, or Ire1α. Knockdown of CHOP reversed the change of diclofenac-induced SNX10 and LAMP2A expression (Figure 32).

Indeed, overexpression of CHOP increased the expression of SNX10 and inhibited the activity of CMA. Knockdown of CHOP reversed the effect of tunicamycin on the expression level of SNX10 and LAMP2A. It also reversed the Nile red fluorescence completely, confirming that CHOP-dependent SNX10 induction is responsible for the lipid accumulation by diclofenac (Figure 33).

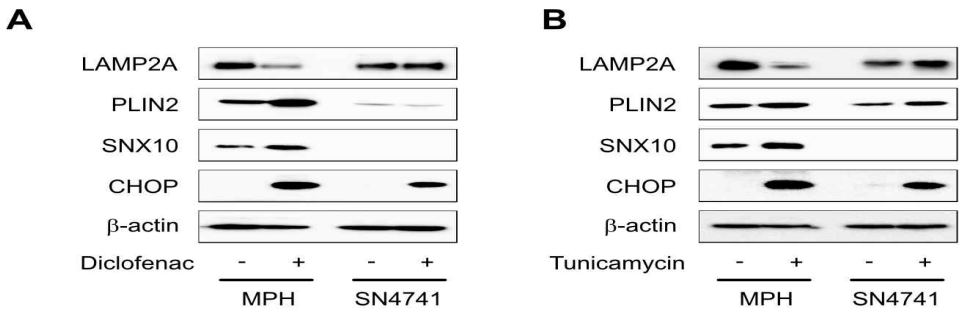

Figure 31. The expression of SNX10 was deficient in SN4741 cells

(A) MPH and SN4741 cells were treated with diclofenac (300 μM) and subjected to western blot analysis with antibodies against LAMP2A, PLIN2, SNX10 and CHOP. (B) MPH and SN4741 cells were treated with tunicamycin (3 μg/ml) and subjected to western blot analysis with antibodies against LAMP2A, PLIN2, SNX10 and CHOP.

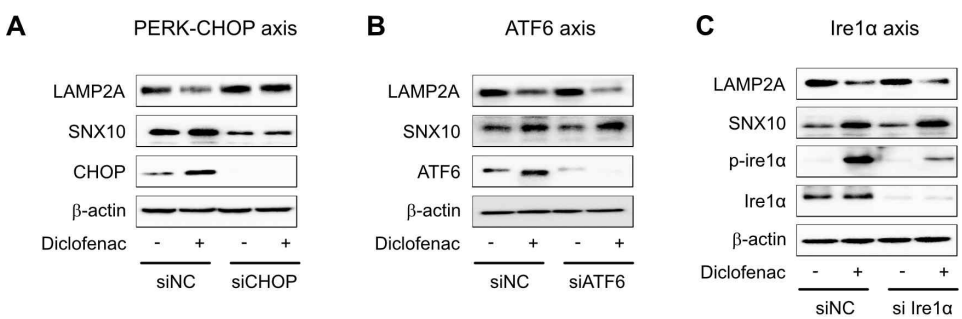

Figure 32. PERK-CHOP pathway regulated SNX10 and LAMP2A expression

(A, B, C) HepG2 cells were transfected with control or CHOP, ATF6, Ire1α siRNA and were incubated with diclofenac (300 μM) for 24 h. The protein levels of LAMP2A, SNX10 were measured by western blot analysis.

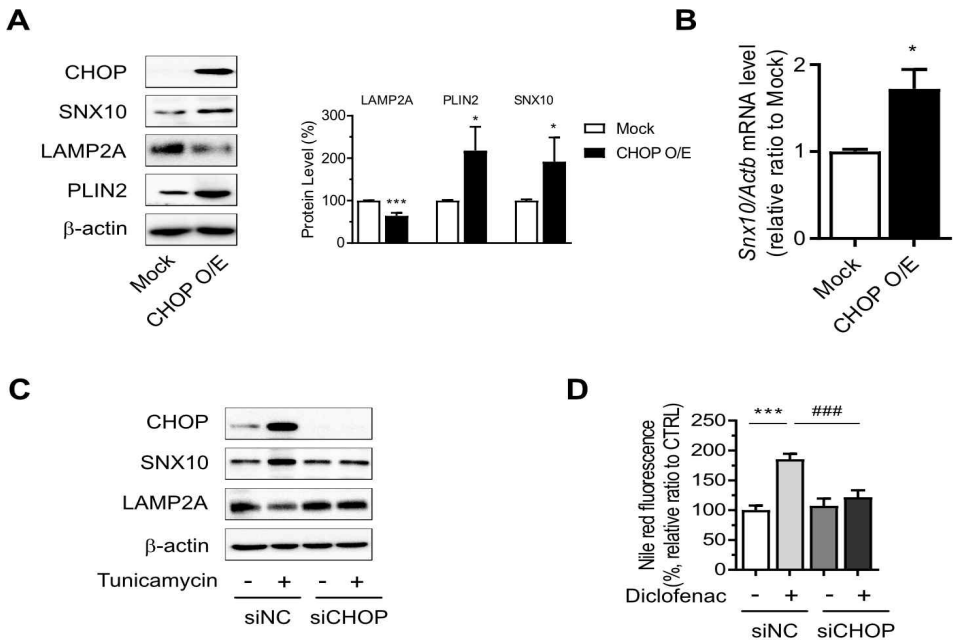

Figure 33. CHOP expression mediated SNX10 upregulation and diclofenac-induced inhibition of CMA.

(A, B) HepG2 cells were transfected with pCMV-CHOP plamsid. (A) The protein levels of CHOP, SNX10, LAMP2A, PLIN2 were measured by western blot analysis. (B) Relative mRNA levels of *Snx10* (C) HepG2 cells were transfected with control or CHOP siRNA and were incubated with tunicamycin for 12 h. The protein levels of CHOP, SNX10, LAMP2A were measured by western blot analysis. (D) HepG2 cells were transfected with control or CHOP siRNA and were incubated with diclofenac for 24 h. Intracellular neutral lipid levels were quantified using Nile-red dye; the excitation and emission wavelengths were 486 and 528 nm, respectively. Data are presented as mean ± SD of at least 3 independent experiments, as analyzed by student's t-test or one-way ANOVA followed by Tuckey's test. *p < 0.05, and ***p < 0.001, relative to the control group. ###p < 0.001, relative to the diclofenac-treated group.

3.7. CMA activator alleviated diclofenac-induced hepatic steatosis *in vivo*

3.7.1. CMA reactivation decreased diclofenac-induced hepatotoxicity and diclofenac-induced lipid accumulation

To establish the role of CMA-dysregulation in diclofenac-induced hepatic steatosis *in vivo*, 7-week-old C57BL/6 mice were intraperitoneally injected with diclofenac and/or AR7, CMA activator by inducing the expression of LAMP2A.

Although there was no difference in body weight or liver-to-body weight ratio, the serum ALT and AST levels revealed significant damage in diclofenac-exposed livers. Co-administration of AR7 abrogated the increase of ALT and AST significantly, which is a biomarker of liver toxicity *in vivo*. Diclofenac injection in mice significantly increased lipid droplets and hepatic lipid accumulation measured by Oil Red O staining and biochemical analysis of TG. CMA activator revealed significant alleviation of hepatic steatosis in the diclofenac and AR7-injected mice (Figure 34).

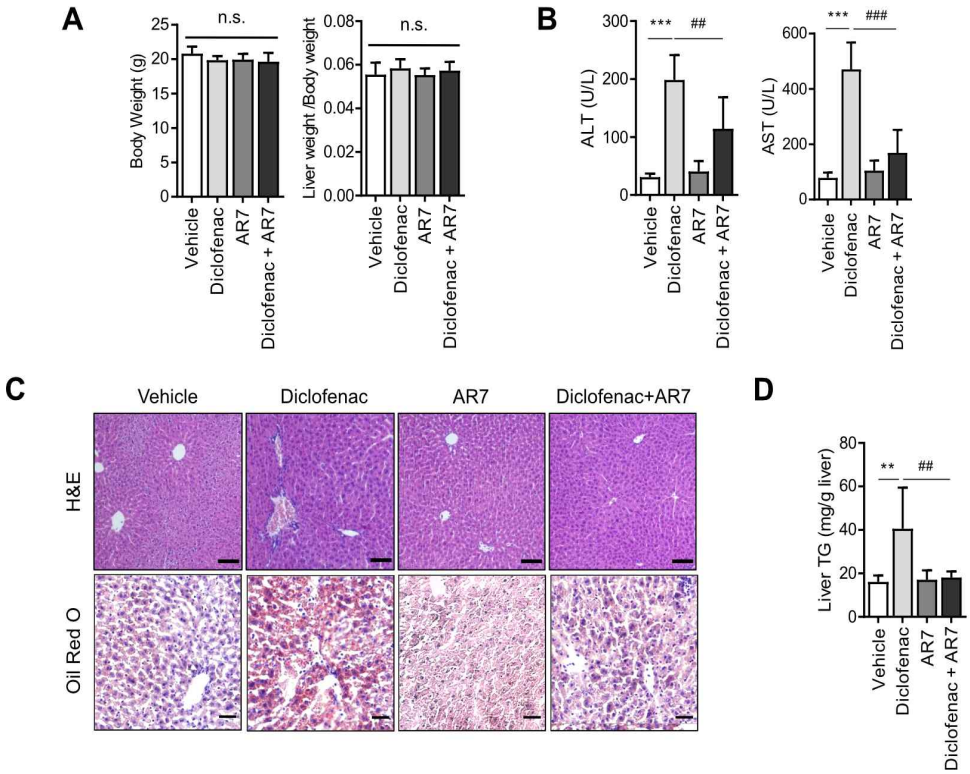

Figure 34. CMA reactivation decreased diclofenac-induced hepatotoxicity and diclofenac-induced lipid accumulation

Male C57BL/6 mice were injected intraperitoneally with AR7 (10 mg/kg) 1 h before diclofenac (100 mg/kg) administration twice every 12h and sacrificed after the final injection. (A) The body weight and liver/body weight ratio are presented. (B) Serum ALT, AST measurements were performed using an automated Chemistry Analyzer (Tokyo Boeki Medical system, Prestige 24I) (C) Histological images of H&E (Scale bars; 100 μm, x20 magnification) and Oil Red O staining of mice liver (Scale bars; 50 μm, x40 magnification). (D) The level of hepatic TG (mg/g liver) is presented. All of the data are mean ± SD of 6 mice per group in *in vivo* experiments, as analyzed

by one-way ANOVA followed by Tuckey's test. **p < 0.01, and ***p < 0.001, relative to the control group. ##p < 0.01, ###p < 0.001, relative to the indicated group. n.s.; non-significant relative to the control group.

3.7.2 CMA activator reduced the accumulation of CMA substrates by diclofenac *in vivo*.

To determine whether diclofenac-induced inhibition of CMA was reversed by CMA activator, LAMP2A and CMA substrates protein were measured. The expression levels of the CMA substrates and LAMP2A were reversed by the administration of AR7 with diclofenac. The levels of Hsc70 did not change in any of the groups. LAMP2A from the liver lysate, as well as from the purified lysosomal fraction, was downregulated by diclofenac injection. As expected, the mRNA levels of LAMP2A and GAPDH were not changed by the administration of diclofenac. On the other hand, the primary target of diclofenac, SNX10, was significantly increased at the transcriptional level by diclofenac administration, which was reversed by AR7 only slightly, not significantly. Expression of SNX10 was increased by diclofenac, followed by elevation of SNX10-mediated CTSA maturation. Administration of AR7 with diclofenac blocked the escalation of SNX10, as well as a mature form of CTSA (Figure 34). Taken together, diclofenac treatment induced liver injury and lipid accumulation *in vivo*, and CMA activation by AR7 alleviated diclofenac-induced hepatic steatosis and toxicity (Figure 35).

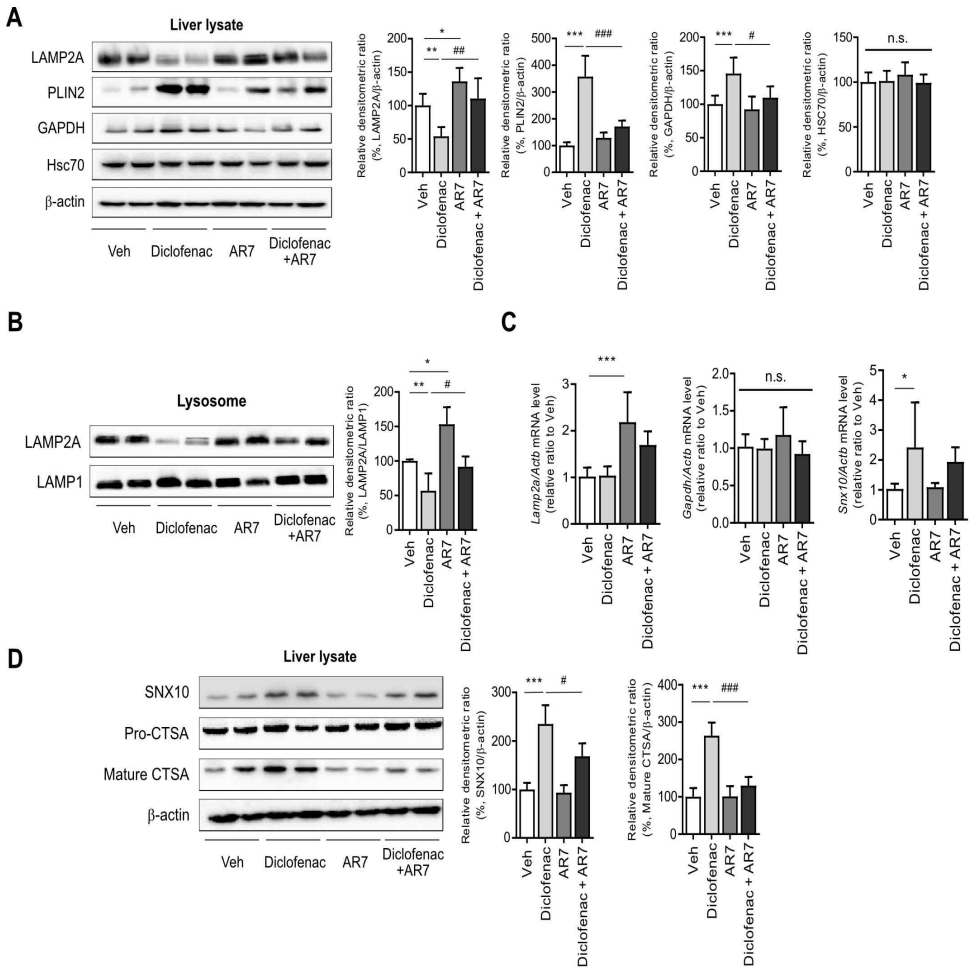

Figure 35. CMA activator reduced the accumulation of CMA substrates by diclofenac *in vivo*.

Male C57BL/6 mice were injected intraperitoneally with AR7 (10 mg/kg) 1 h before diclofenac (100 mg/kg) administration twice every 12h and sacrificed after the final injection. (A) Protein extracts were prepared from mouse liver homogenates, and the protein levels of LAMP2A, PLIN2, GAPDH, and HSC70 were assessed by western blotting. The right panel shows the densitometric quantification of

target proteins. (B) Western blots for LAMP2A protein in a lysosomal fraction of mice liver. (C) mRNA was prepared from mouse livers, and the mRNA levels of *Lamp2a*, *Gapdh*, *Snx10* were assessed by qRT-PCR. (D) Protein extracts were prepared from the liver homogenates and subjected to western blot analysis with antibodies against SNX10, Pro-CTSA, cleaved CTSA. All of the data are mean ± SD of 6 mice per group in *in vivo* experiments, as analyzed by one-way ANOVA followed by Tuckey's test. *$p < 0.05$, **$p < 0.01$, and ***$p < 0.001$, relative to the control group. #$p < 0.05$, ##$p < 0.01$, ###$p < 0.001$, relative to the indicated group. n.s.; non-significant relative to the control group.

4. Discussion

Hepatic lipids increase in many diseases involving disrupted lipid metabolism, including non-alcoholic fatty liver disease, metabolic and immunological diseases. Intracellular lipids are degraded by lipolysis and lipophagy. While LDs in adipocytes are hydrolyzed predominantly by lipases, their expression in non-adipose tissue is relatively low. Therefore, the lysosomal-autophagic pathway plays a critical role in the early steps of lipid degradation in hepatocytes (Settembre *et al.* 2014). PLIN2 is one of the most abundantly expressed lipid droplet (LD) coating proteins and plays a crucial role in maintaining the stability of LD. The degradation of PLIN2 by CMA and subsequent activation of lipolysis or lipophagy are critical cellular pathways of LD catabolism. (Kaushik *et al.* 2015)

Earlier studies have reported that pirprofen and ibuprofen inhibit microsomal β-oxidation of fatty acids and thus induce hepatic microvesicular steatosis (Geneve *et al.* 1987; Freneaux *et al.* 1990). However, there is a lack of understanding on the underlying molecular mechanism of how NSAIDs induce lipid accumulation. The recent study has shown that NSAID-induced lysosomal dysfunction impairs cellular autophagic flux and aggravates an impairment of mitochondrial integrity, which leads to hepatotoxicity (Jung *et al.* 2020). Investigating the possible association of NSAID-induced hepatic abnormal lipid metabolism with autophagy, all tested NSAIDs induced lipid accumulation in hepatocytes NSAIDs including diclofenac inhibit CMA by accelerated degradation of lysosomal LAMP2A, a key regulator of CMA. Impaired CMA activity prevents efficient

degradation of PLIN2, which leads to hepatic lipid accumulation. Diclofenac induced CHOP expression via the ER stress response. CHOP-mediated upregulation of SNX10 facilitated the degradation of LAMP2A via the maturation of CTSA. Here, it was demonstrated for the first time that NSAIDs induce hepatic lipid accumulation via the inhibition of CMA. The results presented in this study provide a new understanding of the role of CMA in drug-induced liver injury and offer new insight into the molecular mechanism of NSAID-induced hepatic steatosis and hepatotoxicity.

CMA is a selective type of autophagy which is mediated by HSC70 chaperone recognition of the KFERQ motif in target proteins. This interaction enables the target proteins to bind the lysosomal receptor called LAMP2A, and the proteins are internalized to the lysosomal lumen (Alfaro *et al.* 2018). LAMP2A is responsible for CMA substrates binding and translocation to the lysosome, and thus CMA activity is determined by the lysosomal level of LAMP2A (Cuervo *et al.* 2000). In the liver, the basal level of LAMP2A and starvation-induced CMA activity is important for the maintenance of lipid homeostasis (Dong *et al.* 2020). Liver-specific conditional knockout mouse for LAMP2A decreases the degradation of liver enzymes related to lipid metabolism, thereby leading to hepatic lipid accumulation (Schneider *et al.* 2014). Likewise, a recent study reported that CMA blockage in macrophages exhibits significant intracellular lipid accumulation (Qiao *et al.* 2021). Conversely, the impairment of CMA has been observed in various metabolic liver diseases. Rodriguez-Navarro *et al.* reported that high lipid content diets reduce CMA activity by increasing the extension of

lipid-enriched microdomains and thus augment lysosomal LAMP2A undergoing degradation (Rodriguez-Navarro *et al.* 2012). Moreover, liver tissues from patients with non-alcoholic fatty liver disease (NAFLD) exhibited a negative relationship between LAMP2A expression and NAFLD steatosis grade (Ma *et al.* 2020). These findings indicate that CMA malfunctioning induced dysregulation of lipid metabolism.

However, there has been limited research on changes in CMA activity following treatment with toxic chemicals. CMA markers including LAMP2A and HSC70 were significantly downregulated in the hepatocytes extracted from rats with D-galactosamine/lipopolysaccharide-induced acute liver failure (Li *et al.* 2017). Conflicting results have been reported regarding the effect of ethanol feeding on CMA activity. Cai *et al.* revealed that chronic ethanol feeding in mice (Leiber-DeCarli model) for 4 weeks impairs CMA activity by reducing HSC70 and LAMP2A in the liver (Cai *et al.* 2016). On the contrary, in another paper, An *in vivo* study of mouse models by You *et al.* pointed out that ethanol feeding increases CMA activity. Still, further activation of CMA by inducing the stability of LAMP2A through liver-specific SNX10 deletion alleviated alcohol-induced liver injury and hepatic steatosis. (You *et al.* 2018).

The molecular structure of the NSAIDs may contribute to hepatic lipid accumulation and CMA inhibition activity. The NSAIDs that induce lipid accumulations in HepG2 cells were either acetic acid or propionic acid derivatives. Diclofenac and other structurally related NSAIDs inhibited CMA by enhanced degradation of lysosomal

LAMP2A. The findings in this study illustrate the essential mechanism by which NSAIDs induce lipid accumulation in the liver.

CMA activity is tightly regulated for the maintenance of cellular homeostasis. As LAMP2A is the main effector of CMA, the level of LAMP2A at the lysosomal membrane is proportional to the activity of CMA (Li *et al.* 2010). The transcription factors identified as modulators of LAMP2A expression were nuclear factor of activated T cells 2 (NFATC2) and nuclear factor erythroid 2-related factor 2 (NRF2) (Valdor *et al.* 2014; Pajares *et al.* 2018). LAMP2A trafficking to the lysosomal membrane or regulation of LAMP2A multimer stability is the key post-transcriptional modulator of LAMP2A level (Zhang *et al.* 2017; Cuervo *et al.* 2003; You *et al.* 2018). Moreover, the dynamics of the LAMP2A translocation complex mediated by glial fibrillary acidic protein (GFAP) and elongation factor 1α (EF1α) are another mechanism of LAMP2A's regulation (Bandyopadhyay *et al.* 2008). Because no significant difference in LAMP2A mRNA level was observed upon treatment of diclofenac, the possibility that NSAIDs manipulate the stability of LAMP2A was explored. Cuervo *et al.* published that a serine protease CTSA determines the stability of monomeric LAMP2A. The mature form of CTSA associates with LAMP2A on the lysosomal membrane and triggers LAMP2A degradation in the lysosome (Cuervo *et al.* 2003). CTSA maturation by diclofenac mediates LAMP2A degradation, leading to CMA inhibition. CTSA knockdown restored LAMP2A expression and attenuated diclofenac-induced hepatic lipid accumulation, supporting the idea that the impairment of CMA activity by NSAIDs results directly from CTSA-mediated degradation of LAMP2A in the liver.

Unlike other cathepsins, CTSA is a lysosomal protease that belongs to the serine proteases family. It makes a complex with the two glycosidases, β-galactosidase (β-gal) and α-neuraminidase (Neu1) to protect them against proteolytic degradation in the lysosome (Timur *et al.* 2016). The LAMP2A-mediated influx into the lysosome precedes the degradation of substrates for CMA, including PLIN2. Since CTSA does not have carboxypeptidase activity at cytoplasmic pH (7.0-7.4), CTSA cannot mediate the degradation of proteins, resulting in the accumulation of CMA substrates in the cytosol. Moreover, it is reported that diclofenac induces lysosomal dysfunction and decreases the activity of Cathepsin B (Jung *et al.* 2020). Although diclofenac increases CTSA activity, the lysosomal activity may have reduced.

The upstream target of diclofenac-induced CTSA maturation was *Snx10* transcription. SNX10 is one of the simplest structure isoforms of sorting nexin family, a family of evolutionarily conserved proteins involved in vesicular trafficking between cellular compartments (Hanley *et al.* 2021). A recent paper demonstrated that SNX10 deficiency alleviated alcoholic liver injury by activating CMA through upregulated transcription and stability of LAMP2A (You *et al.* 2018). This report is consistent with the findings that increased expression of SNX10 by diclofenac ultimately led to hepatic lipid accumulation.

SNX10 expression is expected to be correlated with various liver diseases. To find the correlation between SNX10 and fatty liver disease, the NCBI Gene Expression Omnibus (GEO) database analysis was performed. Microarray data showed that the expression of SNX10 in the mice fed a methionine- and choline-deficient plus

high-fat (MCD+HF) diet, and in the human liver of NAFLD patients was significantly increased (Kita *et al.* 2012; Ahrens *et al.* 2013). Moreover, it is reported that the level of SNX10 is upregulated in human atherosclerotic lesions (You *et al.* 2020). Further research is required to verify the possibility that SNX10 induction in various diseases is implicated in disease development or exacerbation via CMA.

The transcription factors and molecular regulators of SNX10 in the liver are not fully understood. Microarray analysis of the tunicamycin-induced ER stress mouse model reveals the upregulation of SNX10 (Ma *et al.* 2021). In fact, previous studies have shown that ER stress is involved in NSAID-induced toxicity (Liu *et al.* 2019; Tsutsumi *et al.* 2004), where increased intracellular Ca^{2+} level is involved in the upregulation of CHOP (Tanaka *et al.* 2005). Consistent with these findings, all tested NSAIDs significantly increased intracellular Ca^{2+} level and diclofenac upregulated Bip and CHOP in a dose-dependent manner. However, opposing results have also been published that ER stressors activate CMA via p38 MAPK-mediated phosphorylation and stabilization of LAMP2A in the dopaminergic cell line SN4741 (Li *et al.* 2017). Indeed, the expression of SNX10 is deficient, and the level of LAMP2A is not downregulated by diclofenac and tunicamycin in SN4741 cells. These results suggest that SNX10 plays a role in the inhibition of CMA in the liver following ER stress induction. Further studies are needed to clarify the exact role of ER stress in LAMP2A stability and CMA activity.

It has been reported that CMA and macroautophagy compensate each other for protein homeostasis. Changes in the activity of one of

the pathways will affect the contribution of the other pathway to maintain cellular homeostasis (Massey *et al.* 2006). Deletion of Atg5, a macroautophagy-related protein required for autophagosome formation, increases CMA activity (Kaushik *et al.* 2008). CMA blockage for 2 months using LAMP2A RNAi resulted in constitutive activation of macroautophagy. However, CMA blockage for 2 weeks using LAMP2A RNAi inhibited macroautophagy by an impaired fusion of autophagic vacuoles with lysosomes (Massey *et al.* 2008). These results suggest that the effect of CMA blockage on macroautophagy activity depends on the time duration of its inhibition.

In this study, the lipid accumulation effect of diclofenac was independent of the macroautophagy pathway. This is inconsistent with the previous reports that diclofenac inhibits macroautophagy. We estimate that this discrepancy is caused by the difference in concentration of diclofenac used in the experiments. In the present study, CMA activity decreased in response to 200 μM diclofenac exposure. On the other hand, in the previous study, macroautophagy activity decreased after treatment of diclofenac at a concentration of 500 μM (Jung *et al.* 2020).

In our present and previous studies, NSAIDs inhibit both macroautophagy and CMA in hepatocytes. The impairment of macroautophagy by NSAIDs, caused by intracellular ROS and lysosomal dysfunction, prevents the degradation of damaged mitochondria (Jung *et al.* 2020). Concomitant defects of CMA by NSAIDs render cells more susceptible to oxidative stress. (Wang *et al.* 2008). CMA inhibition by NSAIDs induces intracellular lipid

accumulation by inhibiting degradation of the CMA substrate protein, PLIN2. This dual compromise of the two essential autophagy mechanisms may underlie the basis of cellular toxicity following exposure to NSAIDs. Together with the ubiquitin/proteasome system, these autophagy pathways are primarily responsible for cellular homeostasis. Therefore, compromise of the two autophagy pathways can make cells particularly vulnerable to stressors, as they cannot cope with stressor-related damage.

5. Conclusion

The result of the current thesis can be summarized as follows:

First, NSAIDs including diclofenac induced hepatic lipid accumulation *in vitro* and *in vivo*.

Second. NSAIDs increase the abundance of CMA substrates in hepatocytes. NSAIDs inhibit CMA by reducing levels of LAMP2A in the lysosome. The inhibition of CMA by NSAIDs suppressed the degradation of CMA substrates in the lysosome.

Third, CMA reactivation reversed diclofenac-induced failure in the degradation of CMA substrates and reduced diclofenac-induced lipid accumulation in hepatocytes.

Fourth, Inhibition of CMA and subsequent intracellular lipid accumulation by diclofenac is attributed to increased expression of SNX10, activation of CTSA, and, thus, degradation of LAMP2A.

Fifth, CHOP-dependent ER stress response induces SNX10 induction resulting in the CMA inhibition and thus lipid accumulation.

Sixth, CMA activator alleviates diclofenac-induced hepatic steatosis *in vivo*.

Taken together, NSAIDs induced ER stress in the liver, and

CHOP-dependent ER stress response induced SNX10 induction and maturation of CTSA that led to the suppression of CMA activity. Impaired CMA failed to degrade CMA substrates including PLIN2, which ultimately caused the NSAID-induced hepatic steatosis. These results represent a novel insight connecting NSAID overdose to hepatic steatosis.

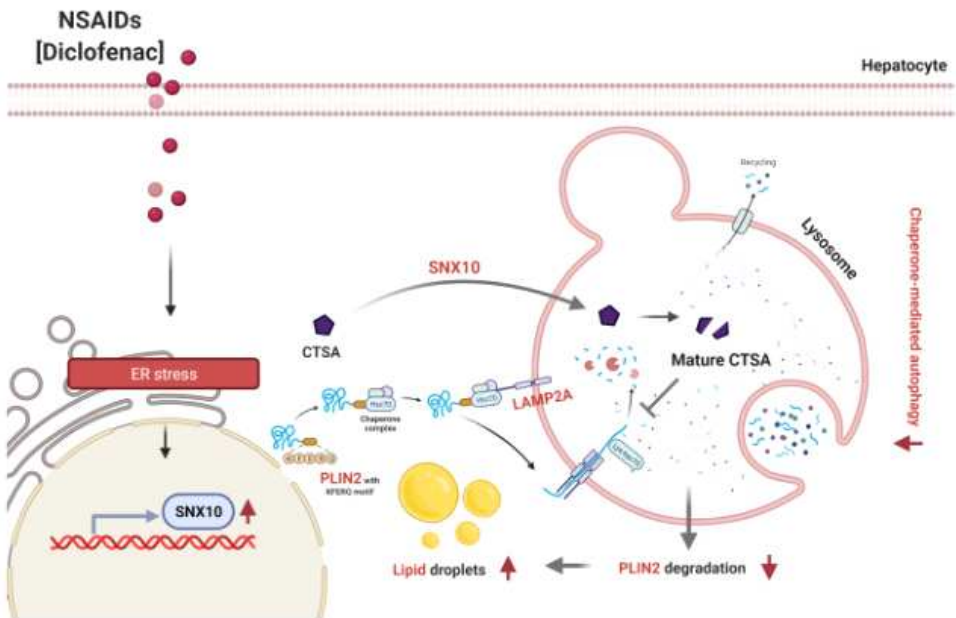

Figure 36. Graphical summary of the mechanism underlying NSAID-induced hepatic steatosis.

6. Reference

Ahrens M., Ammerpohl O., Schönfels W., Kolarova J., Bens S., Itzel T., Teufel A., Herrmann A., Brosch M., Hinrichsen H., Erhart W., Egberts J., Sipos B., Schreiber S., Häsler R., Stickel F., Becker T., Krawczak M., Röcken C., Siebert R., Schafmayer C., Hampe J. (2013) DNA methylation analysis in nonalcoholic fatty liver disease suggests distinct disease-specific and remodeling signatures after bariatric surgery. Cell Metabolism. 18(2):296-302

Agúndez J.G., Lucena M.I., Martínez C., Andrade R.J., Blanca M., Ayuso P., García-Martín E. (2011) Assessment of nonsteroidal anti-inflammatory drug-induced hepatotoxicity. Expert Opinion on Drug Metabolism & Toxicology. 7(7):817-28

Al-Attrache H., Sharanek A., Burban A., Burbank M., Gicquel T., Abdel-Razzak Z., Guguen-Guillouzo C., Morel I., Guillouzo A. (2016) Differential sensitivity of metabolically competent and non-competent HepaRG cells to apoptosis induced by diclofenac combined or not with TNF-α. Toxicology Letters. 258:71-86

Alfaro I.E., Albornoz A., Molina A., Moreno J., Cordero K., Criollo A., Budini M. (2018) Chaperone mediated autophagy in the crosstalk of neurodegenerative diseases and metabolic disorders. Frontiers in Endocrinology. 9:778

Anguiano J., Garner T.P., Mahalingam M., Das B.C., Gavathiotis E.,

Cuervo A.M. (2013) Chemical modulation of chaperone-mediated autophagy by retinoic acid derivatives. Nature Chemical Biology. 9(6):374-82

Auzmendi-Iriarte J., Matheu A. (2021) Impact of chaperone-mediated autophagy in brain aging: neurodegenerative diseases and glioblastoma. Frontiers in Aging Neuroscience. 12:630743

Bandyopadhyay U., Kaushik S., Varticovski L., Cuervo A.M. (2008) The chaperone-mediated autophagy receptor organizes in dynamic protein complexes at the lysosomal membrane. Molecular and Cellular Biology. 28(18):5747-63

Bandyopadhyay U., Sridhar S., Kaushik S., Kiffin R., Cuervo A.M. (2010) Identification of regulators of chaperone-mediated autophagy. Molecular Cell. 39(4):535-47

Bessone F. (2010) Non-steroidal anti-inflammatory drugs: What is the actual risk of liver damage?. World Journal of Gastroenterology. 16(45):5651-61

Cai Y., Jogasuria A., Yin H., Xu M., Hu X., Wang J., Kim C., Wu J., Lee K., Gao B., You M. (2016) The Detrimental Role Played by Lipocalin-2 in Alcoholic Fatty Liver in Mice. The American Journal of Pathology. 186(9): 2417 - 2428.

Corazzari M., Gagliardi M., Fimia G.M., Piacentini M. (2017)

Endoplasmic reticulum stress, unfolded protein eesponse, and cancer cell fate. Frontiers in Oncology. 7:78

Cuervo A.M., Dice J.F. (2000) Regulation of Lamp2a Levels in the Lysosomal Membrane. Traffic. 1(7):570-83

Cuervo A.M., Mann L., Bonten E.J., Alessandra d'Azzo, Dice J.F. (2003) Cathepsin A regulates chaperone-mediated autophagy through cleavage of the lysosomal receptor. EMBO Journal. 22(1): 47 - 59.

Dikic I., Elazar Z. (2018) Mechanism and medical implications of mammalian autophagy. Nature Reviews Molecular Cell Biology 19(6):349-364

Dong H., Czaja M.J. (2011) Regulation of lipid droplets by autophagy. Trends in Endocrinology & Metabolism. 22(6):234-40

Dong S., Aguirre-Hernandez S., Scrivo A., Eliscovich C., Arias E., Bravo-Cordero J.J., Cuervo A.M. (2020) Monitoring spatiotemporal changes in chaperone-mediated autophagy *in vivo*. Nature Communication. 11(1):645

Dromparis P., Paulin R., Stenson T.H., Haromy A., Sutendra G., Michelakis E.D. (2013) Attenuating endoplasmic reticulum stress as a novel therapeutic strategy in pulmonary hypertension. Circulation. 127(1):115-25

Franceschelli S., Moltedo O., Amodio G., Tajana G., Remondelli P. (2011) In the Huh7 hepatoma cells diclofenac and indomethacin activate differently the unfolded protein response and induce ER stress apoptosis. The Open Biochemistry Journal. 5:45-51

Freneaux E., Fromenty B., Berson A., Labbe G., Degott C., Letteron P., Larrey D., Pessayre D. (1990) Stereoselective and nonstereoselective effects of ibuprofen enantiomers on mitochondrial beta-oxidation of fatty acids. Journal of Pharmacology and Experimental Therapeutics. 255(2):529-35.

Geneve J., Hayat-Bonan B., Labbe G., Degott C., Letteron P., Freneaux E., Dinh T.L., Larrey D., Pessayre D.. (1987) Inhibition of mitochondrial beta-oxidation of fatty acids by pirprofen. Role in microvesicular steatosis due to this nonsteroidal anti-inflammatory drug. Journal of Pharmacology and Experimental Therapeutics. 242(3):1133-7

Gómez-Lechón M.J., Ponsoda X., O'Connor E., Donato T., Castell J.V., Jover. R. (2003) Diclofenac induces apoptosis in hepatocytes by alteration of mitochondrial function and generation of ROS. Biochemical Pharmacology. 66(11):2155-67

Hanley S.E., Cooper K.F. (2021) Sorting Nexins in Protein Homeostasis. Cells. 10(1):17

Jackson M.P., Hewitt E.W. (2016) Cellular proteostasis: degradation of

misfolded proteins by lysosomes. Essay in Biochemistry. 60(2):173-180

Jung S.H., Lee W., Park S.H., Lee K.Y., Choi Y.J., Choi S., Kang D., Kim S., Chang T.S., Hong S.S., Lee B.H. (2020) Diclofenac impairs autophagic flux via oxidative stress and lysosomal dysfunction: Implications for hepatotoxicity. Redox Biology. 37:101751

Kaushik S., Massey A.C., Mizushima N., Cuervo A.M. (2008) Constitutive activation of chaperone-mediated autophagy in cells with impaired macroautophagy. Molecular Biology of the Cell. 19(5):2179-92

Kaushik S., Bandyopadhyay U., Sridhar S., Kiffin R., Martinez-Vicente M., Kon M., Orenstein S.J., Wong E., Cuervo A.M., (2011) Chaperone-mediated autophagy at a glance. Journal of Cell Science. 124(4): 495-99

Kaushik S., Cuervo A.M. (2015) Degradation of lipid droplet-associated proteins by chaperone-mediated autophagy facilitates lipolysis. Nature Cell Biology. 17(6):759-70

Kaushik S., Cuervo A.M. (2016) AMPK-dependent phosphorylation of lipid droplet protein PLIN2 triggers its degradation by CMA. Autophagy. 12(2):432-8

Kaushik S., Cuervo A.M. (2018) The coming of age of chaperone-mediated autophagy. Nature Reviews Molecular Cell Biology. 19(6):365-381

Kita Y., Takamura T., Misu H., Ota T., Kurita S., Takeshita Y., Uno M., Matsuzawa-Nagata N., Kato K., Ando H., Fujimura A., Hayashi K., Kimura T., Ni Y., Otoda T., Miyamoto K., Zen Y., Nakanuma Y., Kaneko S. (2012) Metformin prevents and reverses inflammation in a non-diabetic mouse model of nonalcoholic steatohepatitis. PLoS One. 7(9):e43056

Koga H., Martinez-Vicente M., Macian F., Verkhusha V.V., Cuervo A.M. (2011) A photoconvertible fluorescent reporter to track chaperone-mediated autophagy. Nature Communications. 2:386

Li A., Song N., Riesenberg B., Li Z. (2020) The emerging roles of endoplasmic reticulum stress in balancing immunity and tolerance in health and diseases: mechanisms and opportunities. Frontiers in immunology. 10:3154

Li W., Yang Q., Mao Z. (2010) Chaperone-mediated autophagy: machinery, regulation and biological consequences. “Cellular and Molecular Life Science. 68(5):749-63

Li W., Zhu J., Dou J., She H., Tao K., Xu H., Yang Q., Mao Z. (2017) Phosphorylation of LAMP2A by p38 MAPK couples ER stress to chaperone-mediated autophagy. Nature Communications. 8(1):1763

Li Y., Lu L., Luo N., Wang Y., Gao H. (2017) Inhibition of PI3K/AKt/mTOR signaling pathway protects against

d-galactosamine/lipopolysaccharide-induced acute liver failure by chaperone-mediated autophagy in rats. Biomedicine & Pharmacotherapy. 92:544-553.

Lin J.H., Walter P., Yen T.B. (2008) Endoplasmic reticulum stress in disease pathogenesis. Annual Review of Pathology. 3:399-425

Liu X., Green R.M. (2019) Endoplasmic reticulum stress and liver diseases. Liver Research. 3(1):55-64

Ma P., Wang Z., Wang Y., Hou B., Sun J., Tian H., Li B., Shui G., Yang X., Yang X., Qiang G., Liew C.W., Du G. (2021) Integration of metabolomics and transcriptomics reveals ketone body and lipid metabolism disturbance related to ER stress in the liver. Journal of Proteome Research. 20(8):3875-3888

Ma S.Y., Sun K.S., Zhang M., Zhou X., Zheng X.H., Tian S.Y., Liu Y.S., Chen L., Gao X., Ye J., Zhou X.M., Wang J.B., Han Y. (2020) Disruption of Plin5 degradation by CMA causes lipid homeostasis imbalance in NAFLD. Liver International. 40(10):2427-2438

Massey A.C., Kaushik S., Sovak G., Kiffin R., Cuervo A.M. (2006) Consequences of the selective blockage of chaperone-mediated autophagy. Proc Natl Acad Sci. 103(15):5805-10

Massey A.C., Follenzi A., Kiffin R., Zhang C., Cuervo A.M. (2008) Early cellular changes after blockage of chaperone-mediated

autophagy. Autophagy. 4(4):442-56

Meunier L., Larrey D. (2018) Recent advances in hepatotoxicity of non steroidal anti-inflammatory drugs. Annals of Hepatology. 17(2):187-191

Mizushima N., Levine B. (2020) Autophagy in human diseases. The New England Journal of Medicine. 383:1564-1576

Nadanaciva S., Aleo M.D., Strock C.J., Stedman D.B., Wang H., Will Y. (2013) Toxicity assessments of nonsteroidal anti-inflammatory drugs in isolated mitochondria, rat hepatocytes, and zebrafish show good concordance across chemical classes. Toxicology and Applied Pharmacology. 272(2): 272-80.

Pajares M., Rojo A.I., Arias E., Díaz-Carretero A., Cuervo A.M., Cuadrado A. (2018) Transcription factor NFE2L2/NRF2 modulates chaperone-mediated autophagy through the regulation of LAMP2A. Autophagy. 14(8):1310-1322

Patel V., Sanyal A.J., (2013) Drug-induced steatohepatitis. Clinics in Liver Disease. 17(4): 533-46.

Qiao L., Wang H., Xiang L., Ma J., Zhu Q., Xu D., Zheng H., Peng J., Zhang S., Lu H., Chen W., Zhang Y. (2021) Deficient chaperone-mediated autophagy promotes lipid accumulation in macrophage. Journal of Cardiovascular Translational Research.

14(4):661-669

Rodriguez-Navarro J.A. Kaushik S., Koga H., Dall'Armi C., Shui G., Wenk M.R., Paolo G.D., Cuervo A.M. (2012) Inhibitory effect of dietary lipids on chaperone-mediated autophagy. Proceedings of the National Academy of Sciences of the United States of America. 109(12): E705 - E714

Sarah Low E.L., Zheng Q., Chan E., Lim S.G., (2020) Drug induced liver injury: East versus West - a systematic review and meta-analysis. Clinical and Molecular Hepatology. 26(2):142-154

Schmeltzer P.A., Kosinski A.S., Kleiner D.E., Hoofnagle J.H., Stolz A., Fontana R.J., Russo M.W. (2016) Liver injury from nonsteroidal anti-inflammatory drugs in the United States. Liver International, 36(4): 603-9

Schmeltzer P.A. (2019) Drug-Induced Liver Injury Due to Nonsteroidal Anti-inflammatory Drugs. Current Hepatology Reports. 18(3): 294-9

Schneider J.L., Suh Y., Cuervo A.M. (2014) Deficient chaperone-mediated autophagy in liver leads to metabolic dysregulation. Cell Metabolism. 20(3):417-32

Settembre C., Ballabio A. (2014) Lysosome: regulator of lipid degradation pathways. Trends in Cell Biology. 24(12):743-50

Souza S.C., Muliro K.V., Liscum L., Lien P., Yamamoto M.T., Schaffer J.E., Dallal G.E., Wang X., Kraemer F.B., Obin M., Greenberg A.S. (2002) Modulation of hormone-sensitive lipase and protein kinase A-mediated lipolysis by perilipin A in an adenoviral reconstituted system. Journal of Biological Chemistry. 277(10):8267-72

Su M., Guan H., Zhang F., Gao Y., Teng X., Yang W. (2016) HDAC6 regulates the chaperone-mediated autophagy to prevent oxidative damage in injured neurons after experimental spinal cord injury. Oxidative Medicine and Cellular Longevity. 2016:7263736

Sztalryda C., Brasaemleb D.L. (2017) The perilipin family of lipid droplet proteins: Gatekeepers of intracellular lipolysis. Biochimica et Biophysica Acta. 1862(10 Pt B):1221-1232

Tanaka K., Tomisato W., Hoshino T., Ishihara T., Namba T., Aburaya M., Katsu T., Suzuki K., Tsutsumi S., Mizushima T. (2005) Involvement of intracellular Ca2+ levels in nonsteroidal anti-inflammatory drug-induced apoptosis. Journal of Biological Chemistry. 280(35):31059-67

Timur Z.K., Demir S.A., Seyrantepe Y. (2016) Lysosomal cathepsin A plays a significant role in the processing of endogenous bioactive peptides. Frontiers in Molecular Biosciences. 3: 68.

Tsutsumi S., Gotoh T., Tomisato W., Mima S., Hoshino T., Hwang

H., Takenaka H., Tsuchiya T., Mori M., Mizushima T. (2004) Endoplasmic reticulum stress response is involved in nonsteroidal anti-inflammatory drug-induced apoptosis. Cell Death & Differentiation. 11(9):1009-16

Uzi D., Barda L., Scaiewicz V., Mills M., Mueller T., Gonzalez-Rodriguez A., Valverde A.M., Iwawaki T., Nahmias Y., Xavier R., Chung R.T., Tirosh B., Shibolet O. (2013) CHOP is a critical regulator of acetaminophen-induced hepatotoxicity. Journal of Hepatology. 59(3):495-503

Valdor R., Mocholi E., Botbol Y., Guerrero-Ros I., Chandra D., Koga H., Gravekamp C., Cuervo A.M., Macian F. (2014) Chaperone-mediated autophagy regulates T cell responses through targeted degradation of negative regulators of T cell activation. Nature Immunology. 15(11):1046-54

Wang Y., Singh R., Massey A.C., Kane S.S., Kaushik S., Grant T., Xiang Y., Cuervo A.M., Czaja M.J. (2008) Loss of macroautophagy promotes or prevents fibroblast apoptosis depending on the death stimulus. 283(8):4766-77

Ward C., Martinez-Lopez N., Otten E.G., Carroll B., Maetzel D., Singh R., Sarkar S., Korolchuk V.I. (2016) Autophagy, lipophagy and lysosomal lipid storage disorders. Biochimica et Biophysica Acta. 1861(4):269-84

You Y., Li W., Zhang S., Hu B., Li Y., Li H., Tang H., Li Q., Guan Y., Liu L., Bao W., Shen X. (2018) SNX10 mediates alcohol-induced liver injury and steatosis by regulating the activation of chaperone-mediated autophagy. Journal of Hepatology. 69(1):129-141

You Y., Bao W., Zhang S., Li H., Li H., Dang W., Zou S., Cao X., Wang X., Liu L., Jiang H., Qu L., Zheng M., Shen X. (2020) Sorting nexin 10 mediates metabolic reprogramming of macrophages in atherosclerosis through the lyn-dependent TFEB signaling pathway. Circulation Research. 127(4):534-549

Zhang J., Johnson J.L., He J., Napolitano G., Ramadass M., Rocca C., Kiosses W.B., Bucci C., Xin Q., Gavathiotis E., Cuervo A.M., Cherqui S., Catz S.D. (2017) Cystinosin, the small GTPase Rab11, and the Rab7 effector RILP regulate intracellular trafficking of the chaperone-mediated autophagy receptor LAMP2A. Journal of Biological Chemistry. 292(25):10328-10346

국문 초록

비스테로이드성 항염증제 (NSAID) 는 진통, 해열, 소염 작용에 일상에서 널리 사용하는 약물이지만, 위장관 질환 등 다양한 부작용이 보고되는 약물이기도 하다. 특히 몇몇의 NSAID들은 지방간 질환을 유도한다는 것이 예전부터 보고되어 왔고, 일부 약물은 시장에서 철회되었다. 하지만, 아직 정확한 지방간 유발 기전은 밝혀지지 않았다. 따라서 본 연구에서는 NSAID의 지방간 유발 기전에 관한 연구를 진행하였다.

디클로페낙을 포함한 다수의 NSAID 가 간세포에서 공통적으로 지질을 축적 시켰으며, 기전 연구를 위해 선택된 가장 대표적인 약물인 디클로페낙은 마우스에서도 지질축적을 유도하였다. 기존의 연구에서 샤페론-매개 자가포식이 억제되었을 때, 지질 방울을 둘러싸는 단백질이자 샤페론-매개 자가포식의 기질인 Perilipin2 (PLIN2) 가 축적되어, 간에서 지질 축적을 유도한다고 보고되었다. 본 연구진은 대부분의 NSAID가 공통적으로 샤페론-매개 자가포식의 기질인 PLIN2 와 GAPDH를 축적시켰고, 샤페론-매개 자가포식의 주요 단백질인 LAMP2A를 감소시켰다. 샤페론-매개 자가포식 기질 단백질 들이 공통적으로 가지고 있는 모티프인 KFERQ에 mcherry 형광을 붙여 세포에 주입하여 샤페론-매개 자가포식 활성을 확인할 수 있는 리포터를 이용하였을 때, 디클로페낙에 의해 실제로 샤페론-매개 자가포식 활성이 줄어있는 것을 확인하였다.

샤페론-매개 자가포식을 활성화제인 AR7 혹은 LAMP2A 과발현 벡터로 다시 활성화 시켜 주었을 때, 디클로페낙에 의해 유도된

지질 축적이 줄어든 것을 확인할 수 있었다. NSAID에 의해 유도되는 소포체 스트레스는 CHOP에 의해 Sorting Nexin 10 (SNX10) 을 증가시키고, 이는 Cathepsin A (CTSA)의 lysosome 내 활성형을 증가시키고, 이는 lysosome 내 LAMP2A의 분해를 촉진 시켰다. C57BL/6 마우스에 샤페론-매개 활성화제를 투여했을 때, 디클로페낙에 의한 간 내 지질 축적을 감소시켰다.

즉, 디클로페낙에 의한 간 내 지질 축적 진행에서 소포체 스트레스에 의한 SNX10 의 증가가 CTSA의 활성을 증가시켜 LAMP2A의 lysosome 내 분해를 촉진하고, 이는 샤페론-매개 자가포식의 활성을 감소시켜 기질 단백질인 PLIN2의 축적으로 유도하여 지질 축적을 증가시킨다는 것을 규명하였다. 이는 NSAID의 간독성 및 지방간 유도에 새로운 기전을 제시하여 새로운 치료법 및 전략이 될 수 있음을 시사한다.

주요어 : 샤페론-매개 자가포식, 디클로페낙, 지질 대사, 비스테로이드성 항염증제, Perilipin 2, Sorting Nexin 10

학번 : 2015-21890